Materials for Devices

Bartomeu Monserrat

Michaelmas 2023

Contents

Chapter 1

Dielectric materials

A dielectric material is an electrical insulator that becomes polarised under an applied electric field. Dielectric materials host many interesting physical properties and are key in understanding phenomena in areas as diverse as electronics, optics, condensed matter physics, and cell biology. They are also applied to a wide range of technologies, from robotics to digital memories. In this Chapter, we introduce the basic properties of dielectric materials and investigate some of their remarkable properties, including piezoelectricity and ferroelectricity.

1.1 Dielectric properties of materials

Atoms are made of positively charged nuclei and negatively charged electrons. As a result, molecules and materials present a rich spectrum of responses to applied electric fields. In this Section, we explore the basic interaction between electric fields and dielectric materials, a class of materials in which microscopic charges are not allowed to travel freely through the material.

1.1.1 Electric polarisation

An *electric dipole* is defined as two opposite point charges, one of charge $+q$ and the other of charge $-q$, separated by a distance vector $\mathbf{r}$. This system can be characterised by the *electric dipole moment* $\boldsymbol{\mu}$ defined as:

$$\boldsymbol{\mu} = q\mathbf{r}. \tag{1.1}$$

The electric dipole moment is a vector quantity of units [Cm]. Figure 1.1 provides a schematic overview.

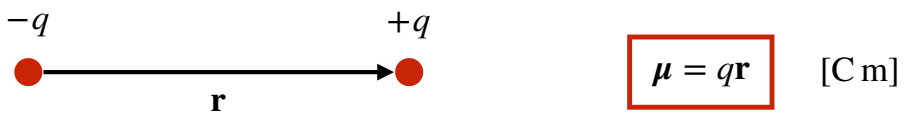

Figure 1.1: Electric dipole moment.

We are often interested in a collection of N electric dipole moments $\boldsymbol{\mu}_i$, where $i = 1, 2, \ldots, N$. The total electric dipole moment $\boldsymbol{\mu}$ is then given by the vector sum of the individual electric dipole moments:

$$\boldsymbol{\mu} = \sum_{i=1}^{N} \boldsymbol{\mu}_i. \tag{1.2}$$

For example, if the individual electric dipole moments all point in random directions, then the total electric dipole moment vanishes, $\boldsymbol{\mu} \simeq 0$. Instead, if the individual electric dipole moments all point in the same direction, and their magnitude $\mu_i = |\boldsymbol{\mu}_i|$ is the same, then the total electric dipole moment is $\boldsymbol{\mu} = N\boldsymbol{\mu}_i$. Both examples are schematically shown in Fig. 1.2.

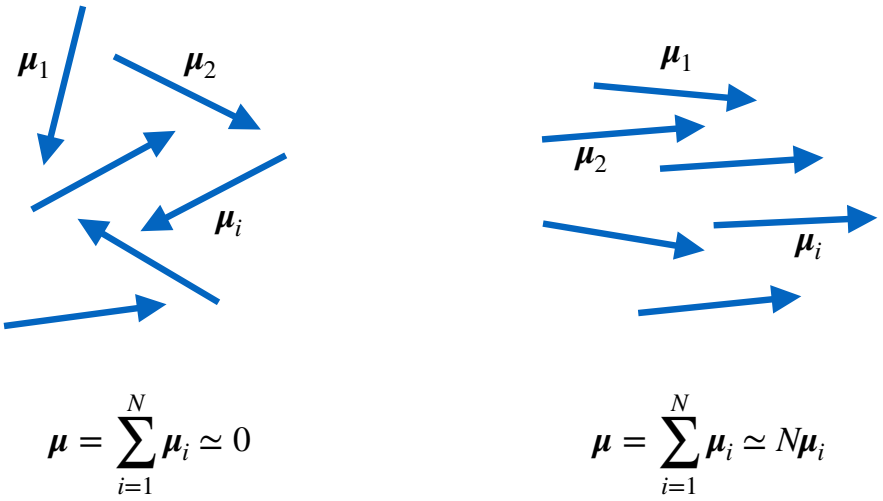

Figure 1.2: Total electric dipole moment for a collection of randomly oriented dipoles (left) and of aligned dipoles (right).

In a material, we define the *polarisation* (also called *polarisation density* or *electric polarisation*) as the density of electric dipole moments. Mathematically, the polarisation $\mathbf{P}$ is given by:

$$\mathbf{P} = n\boldsymbol{\mu}, \tag{1.3}$$

where n is the number of dipoles per unit volume (units $[\mathrm{m}^{-3}]$). The polarisation is a vector quantity of units $[\mathrm{Cm}^{-2}]$.

What is the origin of polarisation in materials? There are multiple microscopic mechanisms that can be responsible for polarisation, for example:

- **Electronic polarisation.** Isolated atoms have a positively charged nucleus (which can be treated as a point charge) and a negatively charged electron cloud around it. In the absence of an electric field, the electron cloud is symmetrically distributed around the nucleus, and there is no net dipole. When an external electric field $\mathbf{E}$ is applied, the electron cloud distorts in the direction opposite to the field, creating an electric dipole moment. This mechanism is depicted in Fig. 1.3. All atoms exhibit electronic polarisation, but electronic polarisation is a small effect in most materials as other polarisation mechanisms dominate. Electronic polarisation dominates in noble gases.

- **Ionic polarisation.** Ionic compounds are materials in which the constituent atoms appear in the form of positive and negative ions. These materials are held together by electrostatic forces between these charges, termed ionic bonding. An example is sodium chloride (NaCl) comprised of sodium cations Na^+ and chloride anions Cl^-. If the ions are symmetrically arranged, the net dipole moment vanishes. If there is a relative displacement of the ions (e.g. driven by the application of an external electric field), an electric dipole moment can develop. This mechanism is depicted in Fig. 1.4.

- **Orientation polarisation.** Molecules with asymmetric charge distributions carry microscopic electric dipole moments, and they are termed polar molecules. An example is

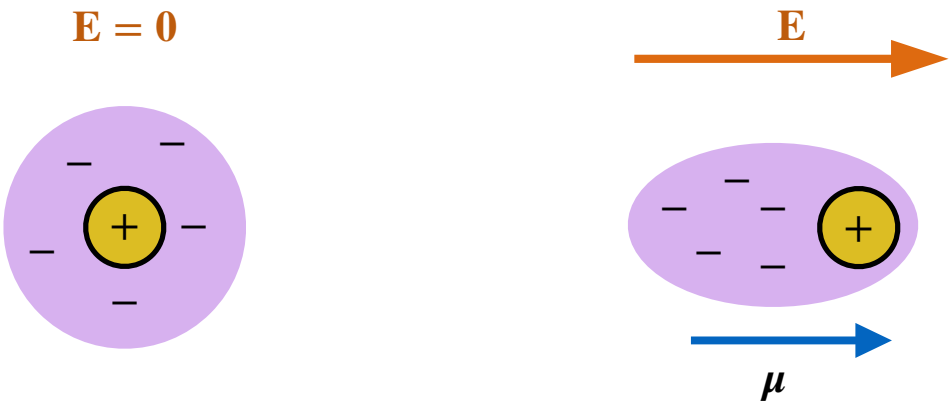

Figure 1.3: Microscopic mechanism for electronic polarisation. There is no electronic dipole moment for an isolated atom (left), but an electronic dipole moment $\boldsymbol{\mu}$ develops in the presence of an external electric field $\mathbf{E}$ (right).

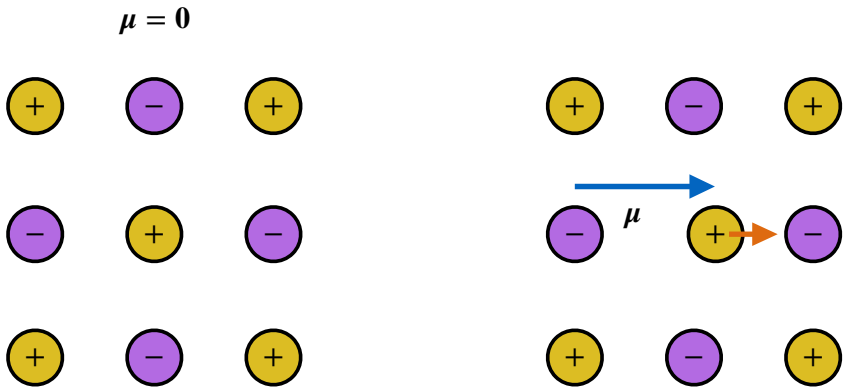

Figure 1.4: Microscopic mechanism for ionic polarisation. There is no electronic dipole moment for symmetrically arranged ions (left), but an electric dipole moment $\boldsymbol{\mu}$ develops if the ions distort from their symmetrical positions (right).

water (H_2O), in which electrons localise around the oxygen atom and away from the hydrogen atoms, resulting in the separation of negative and positive charges forming an electric dipole moment (see Fig. 1.5). These microscopic dipoles may orient randomly (for example due to thermal motion) resulting in zero net polarisation, or they may align (for example by the application of an external electric field) resulting in an overall polarisation. This orientational order mechanism is depicted in Fig. 1.2 with generic dipoles.

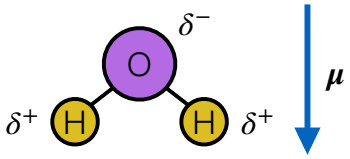

Figure 1.5: Water (H_2O) as a dipolar molecule.

Electronic, ionic, and orientation polarisations are the main microscopic mechanisms responsible for polarisation in materials. In most materials the overall polarisation is typically a combination of these mechanisms.

1.1.2 Dielectric materials

A *dielectric material* is an electrical insulator that can be polarised by an applied electric field $\mathbf{E}$. The induced polarisation $\mathbf{P}$ creates an internal electric field opposite to the externally applied electric field, resulting in a reduced electric field inside the dielectric material. This phenomenology can be characterised by the *displacement field* $\mathbf{D}$, defined as:

$$\mathbf{D} = \varepsilon_0 \mathbf{E} + \mathbf{P}, \tag{1.4}$$

where $\varepsilon_0 = 8.85 \times 10^{-12}\,\mathrm{Fm}^{-1}$ is the *permittivity of free space*. The displacement field has units $[\mathrm{Cm}^{-2}]$, the electric field has units $[\mathrm{Vm}^{-1}]$, and the polarisation has units $[\mathrm{Cm}^{-2}]$. The farad F is the unit of electrical capacitance and is equivalent to 1 coulomb per volt [C/V].

In a linear, homogeneous, and isotropic dielectric material with instantaneous response, the displacement field $\mathbf{D}$ can be related to the applied electric field $\mathbf{E}$ by:

$$\mathbf{D} = \varepsilon \mathbf{E}, \tag{1.5}$$

where ε is the permittivity of the dielectric with units $[\mathrm{Fm}^{-1}]$. Qualitatively, the permittivity of a dielectric material quantifies its electric polarisability: a dielectric with a large permittivity polarises more in response to an applied electric field compared to a material with a low permittivity.

Equation (1.5) holds in a linear, homogeneous, and isotropic dielectric material with instantaneous response. A dielectric material is linear if the permittivity does not depend on the magnitude of the electric field, so that ε is a constant independent of $|\mathbf{E}|$. A dielectric material is homogeneous if its dielectric response is the same at every position inside the material, otherwise ε is a function of the position. A dielectric material is isotropic if its dielectric response is the same in all directions, otherwise ε becomes a tensor. And in a material in which the internal charges do not respond instantaneously to an applied field, then ε becomes frequency dependent. Our focus is on linear, homogeneous, and isotropic dielectric materials with instantaneous response.

There are multiple alternative but equivalent mathematical formulations of the relationship between the displacement field $\mathbf{D}$ and the applied electric field $\mathbf{E}$. A standard formulation uses the permittivity of free space $\varepsilon_0 = 8.85 \times 10^{-12}\,\mathrm{Fm}^{-1}$ to re-write Eq. (1.5) as:

$$\mathbf{D} = \varepsilon \mathbf{E} = \kappa \varepsilon_0 \mathbf{E}, \tag{1.6}$$

where $\kappa = \frac{\varepsilon}{\varepsilon_0}$ is the *dielectric constant* (also called the relative permittivity), a dimensionless quantity.

Comparing Eq. (1.4) with Eq. (1.6), we can write the relationship:

$$\mathbf{P} = \varepsilon_0 \mathbf{E}(\kappa - 1). \tag{1.7}$$

We define the *electric susceptibility* as $\chi = \kappa - 1$, so that we also obtain:

$$\mathbf{P} = \varepsilon_0 \chi \mathbf{E}. \tag{1.8}$$

Qualitatively, the electric susceptibility quantifies the polarisation of a dielectric material in response to an external electric field: a dielectric with a large susceptibitily can be more readily polarised by an external electric field compared to a material with a low susceptibility.

Overall, Eqs. (1.4)–(1.8) provide alternative but equivalent mathematical expressions to describe the response of a dielectric material to an externally applied electric field. Depending on the information available, a given problem will often be more suitably tackled with a specific formulation, so it is useful to become familiar with all.

Table 1.1 provides a few examples of dielectric materials and their dielectric constant. Entries with a range of dielectric constants reflect different external conditions (e.g. temperature) or different microstructure (e.g. defects).

Table 1.1: Examples of dielectric materials and their dielectric constants.

Material	**Dielectric constant** κ
Vaccum	1
Air	1.0006
Paper	1.4
Glass	3.7–10
Water	50–90
$BaTiO_3$	1,200–10,000
$CaCu_3Ti_4O_{12}$	10,000–300,000

1.1.3 An example: parallel plate capacitor

A *capacitor* is an electronic device that stores electrical energy. It is made of two conducting plates separated by a dielectric material, and Fig. 1.6 shows a schematic example of a parallel plate capacitor.

In a charged capacitor, charges of magnitude Q and opposite sign accumulate at each plate, resulting in an electric field $\mathbf{E}$ and associated voltage difference V between the plates. A capacitor is characterised by its *capacitance* C, defined as:

$$C = \frac{Q}{V}. \tag{1.9}$$

The unit of capacitance is the farad [F], and is equivalent to $[CV^{-1}]$.

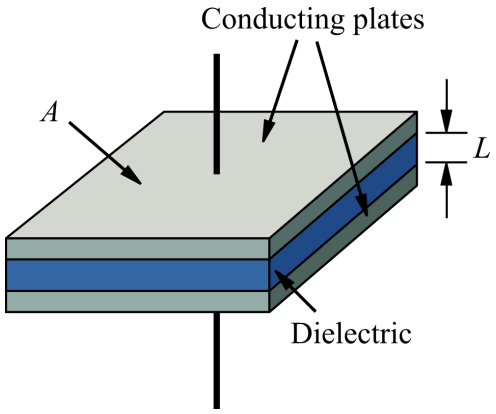

Figure 1.6: Schematic diagram of a parallel plate capacitor. Adapted from Wikipedia.

A parallel plate capacitor is made of two parallel metallic plates of area A and separated by a distance L (Fig. 1.6). The charge Q on the plates can be characterised by the charge density $\sigma = \frac{Q}{A}$. In this setup, the charge density on the plates is equal to the magnitude of the displacement field of the dielectric material between the plates:

$$\sigma = |\mathbf{D}|. \tag{1.10}$$

The derivation of Eq. (1.10) is detailed in Appendix A. Using this result, we obtain:

$$C = \varepsilon \frac{A}{L}. \tag{1.11}$$

The derivation of Eq. (1.11) is detailed in Problem 1.

Equation (1.11) implies that the capacitance of a parallel plate capacitor depends on two quantities: (i) the geometry of the capacitor, and (ii) the dielectric material between the conducting plates. The geometry of the capacitor is characterised by the area A of the plates and

the distance L between the plates. The dielectric material between the conducting plates is characterised by its permittivity ε. If the parallel plate capacitor is in vacuum or air, then $\varepsilon \simeq \varepsilon_0$. If a dielectric material is inserted between the parallel plates, then $\varepsilon > \varepsilon_0$. As $C \propto \varepsilon$, a capacitor can store more electrical energy when its parallel plates are separated by a dielectric material compared to air or vacuum.

1.2 Symmetry and polarisation

The macroscopic properties of materials depend on their microscopic structure. Indeed, unravelling these structure-property relationships is a key endeavour in materials science, physics, and chemistry. In this Section, we discuss how the precise arrangement of atoms in a material, characterised by their symmetry, determines their dielectric response.

1.2.1 Inversion symmetry and polar materials

A *polar material* is a material with a net polarisation. Whether a material is polar or not is closely linked to its structure, and in this section we explore the relationship between polar materials and structural symmetry.

Consider a Cartesian coordinate system. An inversion about the origin of the coordinate system corresponds to the transformation that reflects all points in space about the origin. Mathematically, an inversion transforms a position vector $\mathbf{r}$ in the following manner:

$$\mathbf{r} \longmapsto -\mathbf{r}. \tag{1.12}$$

In terms of Cartesian coordinates, this becomes:

$$(x, y, z) \longmapsto (-x, -y, -z). \tag{1.13}$$

If an inversion operation about a point leaves a geometric structure invariant, then we call the corresponding point an *inversion centre* and we say that the geometric structure has *inversion symmetry* about that point. Figure 1.7 shows two examples of geometric structures that are left invariant under an inversion operation, with the inversion centre located a the origin of coordinates.

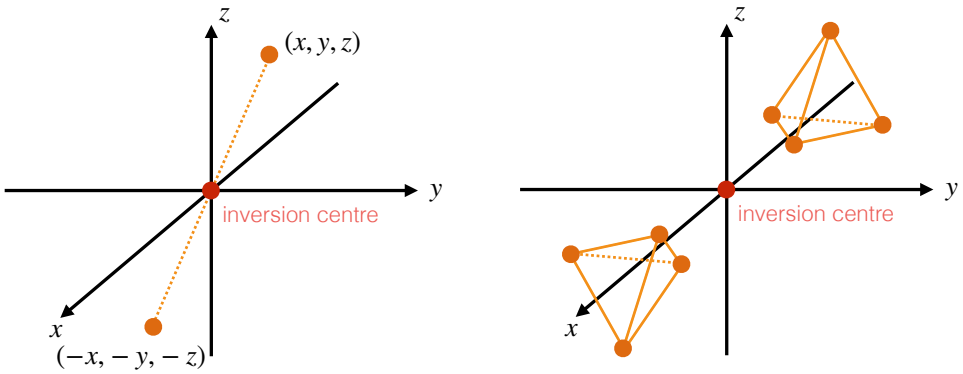

Figure 1.7: Schematic representation of two sets of points exhibiting inversion symmetry. The left diagram shows a single point and its inversion partner and the right diagram shows four points forming the vertices of a tetrahedron and its inversion partner.

If an inversion operation about a point leaves a material invariant, then that point is an inversion centre for the material and we say that the material is *centrosymmetric*. Examples of centrosymmetric materials include diamond and rock salt (NaCl). An electric dipole moment $\boldsymbol{\mu}$ reverses direction under inversion because it is a vector quantity (see example in Fig. 1.8). As a

result, any electric dipole moment in a centrosymmetric material will always have a partner in the opposite direction, implying that centrosymmetric materials cannot be polar materials.

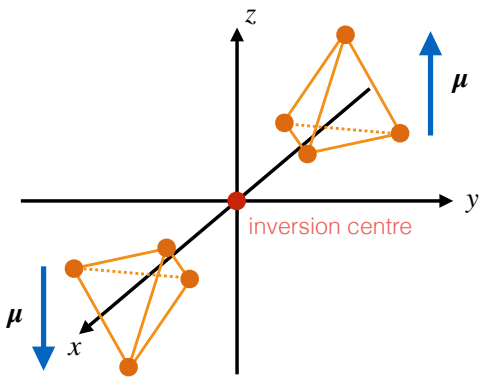

Figure 1.8: Schematic representation of an electric dipole moment $\boldsymbol{\mu}$ associated with a tetrahedral structure and its inversion partner with the electric dipole moment in the opposite direction.

A material without an inversion centre is called a *non-centrosymmetric* material. An example of a non-centrosymmetric material is zinc sulfide (ZnS). It exists in two main crystalline forms (called polymorphs) in the zincblende (Fig. 1.9) and wurtzite (Fig. 1.10) structures, and both are non-centrosymmetric. The electronic configuration of sulfur S is $[\mathrm{Ne}]3s^2 3p^4$ and that of zinc Zn is $[\mathrm{Ar}]3d^{10}4s^2$, so that together they form an ionic compound with S^{2-} and Zn^{2+} ions. Given the ionic nature of the compound and the lack of an inversion centre, a natural question to ask is whether these compounds are polar.

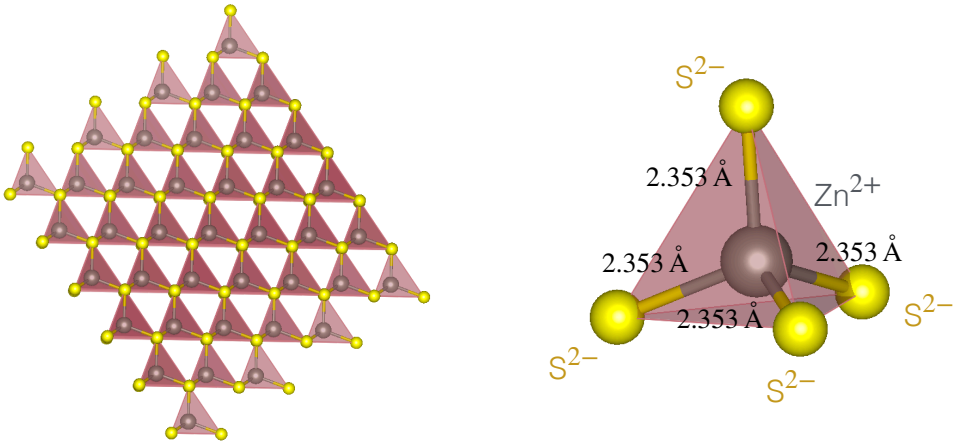

Figure 1.9: ZnS in the zincblende structure (left) and the corresponding perfect tetrahedral building block (right).

Let us first consider ZnS in the zincblende structure as shown in Fig. 1.9. The zincblende structure is a face centred cubic (fcc) structure with two atoms in the primitive cell. A convenient way to analyse the structure is to consider the tetrahedron shown on the right hand side of Fig. 1.9 as its building block. In this tetrahedron, S atoms form the vertices and a Zn atom is at the centre. In the zincblende structure, each S atom is shared between four equivalent tetrahedra, and therefore each S atom only contributes 1/4 of its ionic charge to a given tetrahedron, and as a result each tetrahedron is charge neutral. Additionally, the Zn atom sits at the centre of the tetrahedron and all bond lengths are equal. This symmetric distribution of positive and negative ions implies that there is no net dipole moment in the tetrahedron, and ZnS in the zincblende structure is not a polar material.

Let us next consider ZnS in the wurtzite structure as shown in Fig. 1.10. The wurtzite

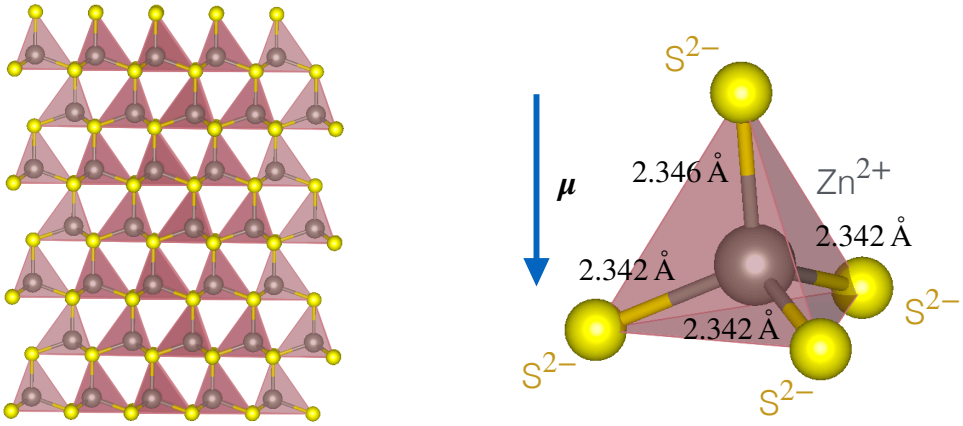

Figure 1.10: ZnS in the wurtzite structure (left) and the corresponding distorted tetrahedral building block (right).

structure is a hexagonal structure with four atoms in the primitive cell and whose building block is the tetrahedron shown on the right hand side of Fig. 1.10. Differently from the zincblende structure, in the wurtzite structure the central Zn atom is not located at the centre of the tetrahedron, leading to the elongation of one bond length compared to the other three. This leads to an asymmetric distribution of positive and negative ions such that an electric dipole moment develops in the tetrahedron. Combining all tetrahedra, ZnS in the wurtzite structure is a polar material.

Overall, a systematic study of the symmetries of crystal structures allows us to classify materials according to their polarity. There are 32 crystal classes (also called point groups), of which 11 are centrosymmetric and 21 are non-centrosymmetric. The 11 centrosymmetric crystal classes lead to non-polar materials. Of the 21 non-centrosymmetric crystal classes, 11 are non-polar and 10 are polar.

In this section we have described the classification of crystal classes into centrosymmetric and non-centrosymmetric, and the latter into polar and non-polar. This classification allows us to characterise the polarity of crystalline materials at equilibrium. In the following sections, we explore how we can modify the polarity of a material using external stimuli including stress, temperature, and electric fields.

1.2.2 Piezoelectric materials

Piezoelectricity refers to the change in electric dipole moment driven by the application of mechanical stress. Centrosymmetric materials are not piezoelectric as inversion symmetry counteracts any local changes in dipoles driven by mechanical stress. Both polar and non-polar non-centrosymmetric materials are piezoelectrics [1]. In a polar non-centrosymmetric material, piezoelectricity implies that the application of mechanical stress changes the magnitude or direction of the polarisation. In a non-polar non-centrosymmetric material, piezoelectricity implies that the application of mechanical stress creates a polarisation in the material.

As an example, consider a piezoelectric material in the form of a rectangular prism. The application of external forces as indicated in Fig. 1.11 leads to a mechanical stress T that drives a piezoelectric response. We analyse this response in the direction parallel to the applied forces. In this one-dimensional model, the piezoelectric effect is characterised through the displacement

[1] In fact there is an exception to this statement. Of the 21 non-centrosymmetric crystal classes, only 20 are actually piezoelectric. One of the non-centrosymmetric cubic crystal classes, called gyroidal, is not piezoelectric. In this crystal class, the existing symmetries are such that any local change in dipoles is counteracted, just like in a centrosymmetric material, despite the lack of an inversion centre.

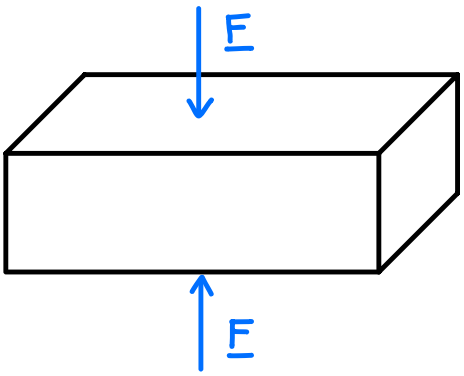

Figure 1.11: Schematic diagram of stress applied to a rectangular prism.

field D by:

$$D = \varepsilon E + dT, \tag{1.14}$$

where, as usual, ε is the permittivity and E is the electric field, and d is called the piezoelectric coefficient. Note that d has units $[\mathrm{CN}^{-1}]$ and T has units $[\mathrm{Nm}^{-2}]$. The first term in Eq. (1.14) is the usual relationship between the displacement field and the electric field, and the second term characterises the further changes driven by the applied stress T, quantified by the piezoelectric coefficient d. As there is no free charge in our setup, from Gauss's law we conclude that $D = 0$. From standard electrostatics, the relationship between electric field E and potential difference ΔV across the length L of the prism is given by $E = -\frac{\Delta V}{L}$. Combining these relationships with Eq. (1.14), we obtain:

$$\Delta V = \frac{dTL}{\varepsilon}. \tag{1.15}$$

This equation gives the change in voltage ΔV generated across the prism with the application of a stress T. It is proportional to the piezoelectric coefficient d and to the length of the prism L, and inversely proportional to the permittivity ε.

The piezoelectric effect as described so far, the change in polarity driven by an external mechanical stress, is the so-called "direct" or generator piezoelectric effect. Piezoelectric materials also host the opposite effect, the mechanical deformation of the material under the application of an electric field, called the "converse" or motor piezoelectric effect.

Piezoelectrics materials find multiple technological applications. The direct piezoelectric effect is used in igniters, energy harvesting, flashlights on trainers, and many others. The converse piezoelectric effect is used in watches, hexapods, and many others.

1.2.3 Pyroelectric materials

Pyroelectricity refers to the change in electric dipole moment driven by a temperature change. Specifically, increasing temperature drives thermal expansion of materials, which in turn can modify their electric dipole moments. Thermal expansion does not change the relative position of the positive and negative centres of charge in centrosymmetric and non-polar non-centrosymmetric materials. Therefore, non-polar materials are not pyroelectric. Thermal expansion does change the relative position of the positive and negative centres of charge in non-centrosymmetric polar materials. Therefore, polar materials are pyroelectric. Indeed, polar materials and pyroelectric materials are often used as synonyms.

Pyroelectric materials find multiple technological applications, examples including infrared detectors and thermal imaging cameras.

1.2.4 Ferroelectric materials

Ferroelectric materials are polar materials whose polarisation direction can be changed by the application of an external electric field. All ferroelectric materials are also polar (pyroelectric) materials, but not all polar materials are ferroelectric.

Ferroelectric materials have historically played a key role in both fundamental science and technological applications. For this reason, we explore their properties in detail in the next section.

1.3 Ferroelectric materials

Ferroelectricity is a physical phenomenon that has played a prominent role in both the development of fundamental science and in technological progress. In this Section, we discuss some key ideas associated with ferroelectricity, ranging from fundamental science in the form of second-order phase transitions, to applied science in the form of hysteresis loops.

1.3.1 The perovskite structure

The mineral calcium titanium oxide ($CaTiO_3$) is called perovskite after mineralogist Lev Perovski. Many other compounds with stoichiometry ABX_3 adopt this same structure, which is referred to as the *perovskite structure*. In the perovskite structure, atoms A and B are positive ions (cations) while X is a negative ion (anion), typically oxygen. Many ferroelectrics adopt the perovskite structure, with barium titanate ($BaTiO_3$) being a prominent example.

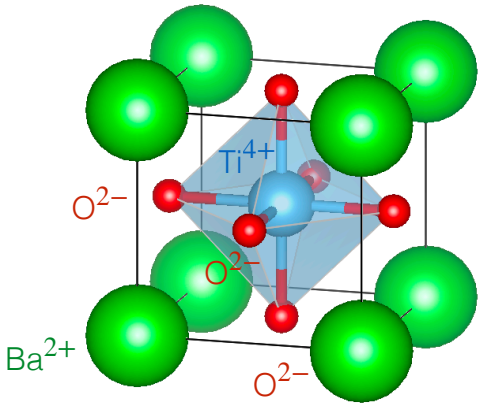

Figure 1.12: The structure of cubic $BaTiO_3$.

The cubic perovskite structure of $BaTiO_3$ is depicted in Fig. 1.12. The primitive cell is cubic, with lattice parameters $a = b = c$ and angles $\alpha = \beta = \gamma = 90°$, and a five atom basis with one barium Ba atom, one titanium Ti atom, and three oxygen O atoms. In the primitive cell depicted in Fig. 1.12, the Ba atoms sit at the corners of the cube and each is shared amongst eight different cells, while the O atoms sit at the faces of the cube and each is shared amongst two different cells. The central Ti is surrounded by six O atoms, which form the corners of a regular octahedron. $BaTiO_3$ is an ionic compound, with cations Ba^{2+} and Ti^{4+} and anions O^{2-}, but the cubic perovskite structure is centrosymmetric and therefore non-polar.

The perovskite structure often distorts from the ideal cubic form depicted in Fig. 1.12. These distortions can be characterised by a simple indicator, called the *Goldschmidt tolerance factor*:

$$t = \frac{r_A + r_X}{\sqrt{2}(r_B + r_X)}, \tag{1.16}$$

where r_A, r_B, and r_X are the ionic radii of ions A, B, and X, respectively. The derivation of Eq. (1.16) is detailed in Problem 3. Qualitatively, the Goldschmidt tolerance factor t quantifies

how well the ions can pack together in the perovskite structure, with $t = 1$ indicating that the cubic structure is favoured, $t > 1$ indicating that the A cations are too large, and $t < 1$ indicating that the B cations are too large.

For $BaTiO_3$, the ionic radii are $r_A = r_{Ba^{2+}} = 1.75\,\text{Å}$, $r_B = r_{Ti^{4+}} = 0.75\,\text{Å}$, and $r_X = r_{O^{2-}} = 1.21\,\text{Å}$. This gives a Goldschmidt tolerance factor of $t \simeq 1.07$, which indicates that the Ba^{2+} cations are too large for ideal packing. This implies that the $BaTiO_3$ structure is larger than ideal to accommodate the Ba^{2+} cations, leaving empty space around the comparatively smaller Ti^{4+} cations. As a result, the Ti^{4+} cations are relatively free to move from their ideal position at the centre of the octahedron, driving distortions from the ideal cubic phase in $BaTiO_3$.

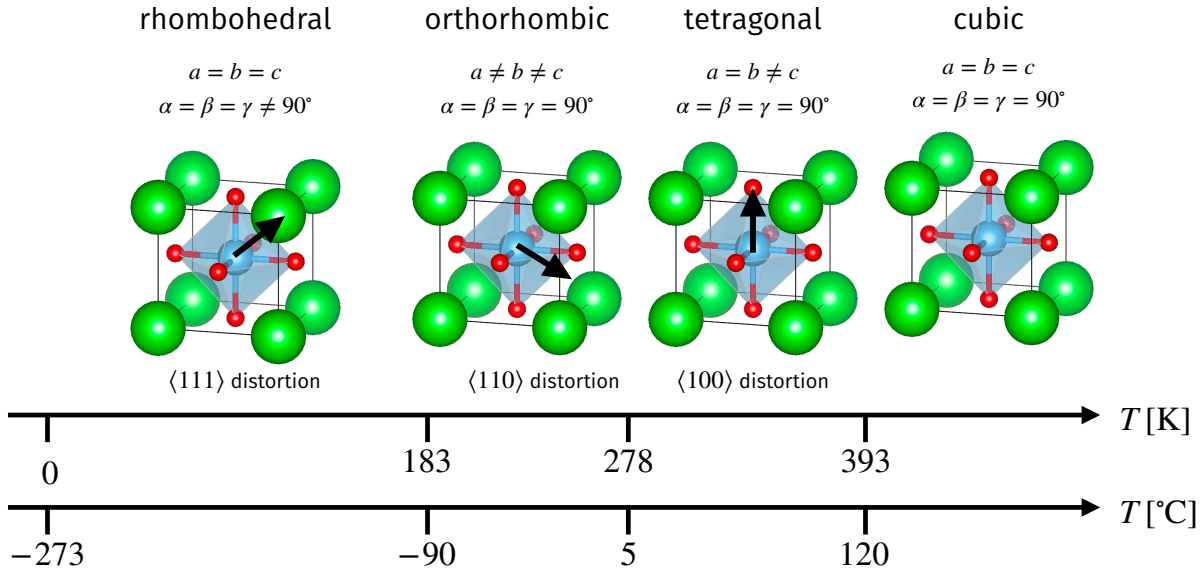

Figure 1.13: Structural phase diagram of $BaTiO_3$ as a function of temperature.

As suggested by its Goldschmidt tolerance factor $t > 1$, $BaTiO_3$ undergoes structural distortions from the ideal cubic perovskite structure driven by the motion of the Ti^{4+} cations. $BaTiO_3$ exhibits a total of four distinct structural phases as a function of temperature, as schematically depicted in Fig. 1.13. At high temperature $T > 393\,\text{K}$, $BaTiO_3$ adopts the ideal cubic perovskite structure. For lower temperatures, the Ti^{4+} cations distort along the $\langle 100 \rangle$ direction (there are 6 possible equivalent directions) with an associated elongation of the primitive cell, resulting in a tetragonal structure. The tetragonal structure exists in the temperature range $278\,\text{K} < T < 393\,\text{K}$. At even lower temperatures, the Ti^{4+} cations instead distort along the $\langle 110 \rangle$ direction (there are 12 possible equivalent directions) and the resulting structure is orthorhombic, stable in the temperature range $183\,\text{K} < T < 278\,\text{K}$. Finally, at temperatures $T < 183\,\text{K}$, the Ti^{4+} cations distort along the $\langle 111 \rangle$ direction (there are 8 equivalent directions) and the resulting structure is rhombohedral.

The cubic $BaTiO_3$ structure is centrosymmetric and non-polar. The centre of positive charge, arising from the Ba^{2+} and Ti^{4+} cations, coincides with the centre of negative charge arising from the O^{2-} anions, and in the choice of primitive cell depicted in the left diagram of Fig. 1.14 it can be assigned to the centre of the octahedron. The tetragonal, orthorhombic, and rhombohedral $BaTiO_3$ structures are non-centrosymmetric and polar. For example, in the tetragonal structure the Ti^{4+} cation moves along the $\langle 100 \rangle$ direction (see examples in the central and right diagrams of Fig. 1.14), displacing the centre of positive charge relative to the centre of negative charge. As a result, an electric dipole moment appears in the tetragonal phase. As depicted in the central and right diagrams of Fig. 1.14, the electric dipole moment can point in different directions depending on the distortion direction of the Ti^{4+} cation. As there are 6 different but equivalent $\langle 100 \rangle$ directions, there are 6 different directions in which the electric dipole moment can point

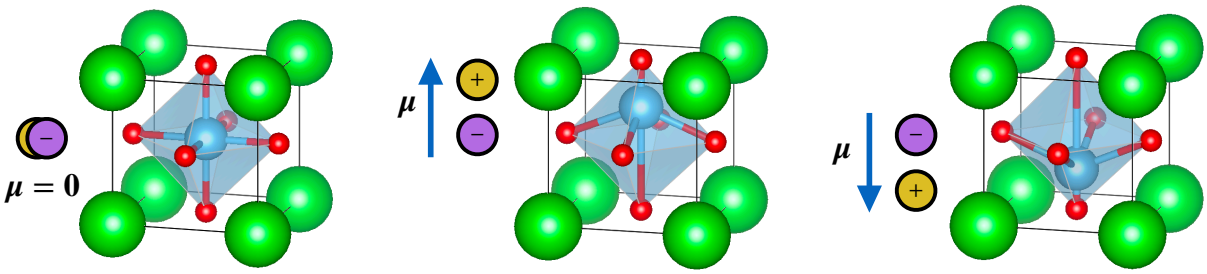

Figure 1.14: The structure and centres of positive and negative charge of the cubic (left) and tetragonal (centre and right) phases of $BaTiO_3$.

in the tetragonal phase of $BaTiO_3$.

$BaTiO_3$ in the polar phases is a ferroelectric material. This means that the polarisation direction can be changed by the application of an external electric field in the appropriate direction. Furthermore, this means that the cubic-to-tetragonal structural phase transition is also a paraelectric-to-ferroelectric phase transition. We investigate this phase transition in more detail next.

1.3.2 Landau theory

Many materials undergo temperature-driven structural phase transitions such as those exhibited by $BaTiO_3$ (Fig. 1.13). Physicist Lev Landau introduced a general phenomenological theory to describe phase transitions, and in this section we will illustrate the basic principles of Landau theory with the discussion of a paraelectric-to-ferroelectric phase transition.

From thermodynamics, the most stable structure at temperature T is the one that minimises the Helmholtz free energy:

$$\mathcal{F} = U - TS, \tag{1.17}$$

where U is the internal energy and S is the entropy. In general, it is rather difficult to evaluate the Helmholtz free energy for a given material. Instead, Landau theory uses basic principles such as the symmetry of the material to build a phenomenological expression for the free energy.

To build such a theory for a paraelectric-to-ferroelectric phase transition in an ionic crystal, we can consider the relative displacement of the anions and cations. In the case of $BaTiO_3$, this would be the position of the Ti^{4+} cation. We consider a coordinate system with origin at the centre of the octahedron, and the Ti^{4+} distortion along the z direction as depicted in Fig. 1.14. In the cubic non-polar phase, Ti^{4+} is at the centre of the octahedron ($z = 0$) and in the tetragonal phase it moves in the positive or negative z direction. This means we could describe the Helmholtz free energy as a function of z. However, the polarisation is proportional to the displacement, and it is conventional to describe the Helmholtz free energy as a function of P instead [2]. In this context, P is called the *order parameter* characterising the phase transition.

Within Landau theory, we write the free energy as:

$$\mathcal{F}(P,T) = a(T - T_c)P^2 + \frac{b}{2}P^4. \tag{1.18}$$

The scalars a and b are positive parameters whose values can be fitted to relevant data for the material of interest. The critical temperature T_c marks the transition temperature between the two phases. Equation (1.18) provides a general description of second order phase transitions. Some paraelectric-to-ferroelectric phase transitions are second order, and we will investigate their properties below. The cubic-to-tetragonal paraelectric-to-ferroelectric transition in $BaTiO_3$ is

[2] The polarisation $\mathbf{P}$ is a vector, but in our example it is parallel to the z direction and therefore we can use its scalar component along that direction.

instead a first-order phase transition, which can also be described within Landau theory, but it requires including an additional term proportional to P^6 in the free energy.

Problem 4 provides a detailed study of Landau theory for second order phase transitions, and here we summarise the main results. The polarisation at temperature T is given by:

$$\begin{cases} P = 0 & \text{for } T > T_\mathrm{c}, \\ P = \pm\sqrt{\frac{a}{b}(T_\mathrm{c} - T)} & \text{for } T < T_\mathrm{c}. \end{cases} \tag{1.19}$$

For $T > T_\mathrm{c}$, the free energy $\mathcal{F}(P,T)$ has a single minimum at $P = 0$, which corresponds to the non-polar phase. For $T < T_\mathrm{c}$, the free energy $\mathcal{F}(P,T)$ has two minima at two non-zero values $P = \pm\sqrt{\frac{a}{b}(T_\mathrm{c} - T)}$, corresponding to the two possible and opposite polarisation directions in the polar phase. Equation (1.19) is depicted in Fig. 1.15, showing that the polarisation decreases with increasing temperature until it vanishes at $T = T_\mathrm{c}$. In a first order phase transition, the polarisation also decreases with increasing temperature, but it does not continuously go to zero, instead it discontinuously jumps from a finite value below T_c to zero above T_c.

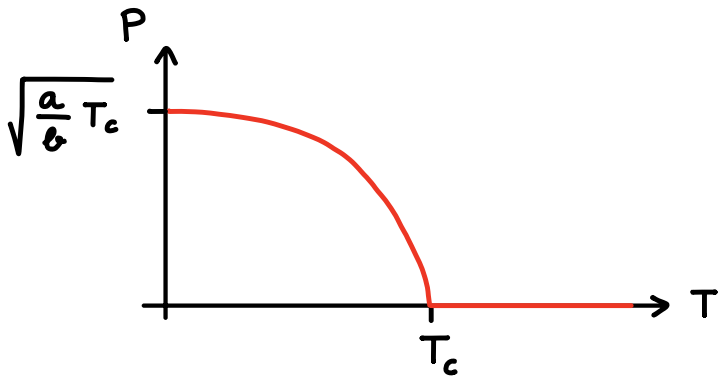

Figure 1.15: Schematic of the polarisation as a function of temperature.

We can extend Landau theory to consider the effect of an external electric field E parallel to the polarisation direction:

$$\mathcal{F}(P,T) = a(T - T_\mathrm{c})P^2 + \frac{b}{2}P^4 - EP. \tag{1.20}$$

Problem 5 provides a detailed study of Eq. (1.20), and here we summarise the main results. The electric susceptibility χ is given by:

$$\begin{cases} \chi = \frac{1}{2a\varepsilon_0(T - T_\mathrm{c})} & \text{for } T > T_\mathrm{c}, \\ \chi = -\frac{1}{4a\varepsilon_0(T - T_\mathrm{c})} & \text{for } T < T_\mathrm{c}. \end{cases} \tag{1.21}$$

Remember that the electric susceptibility quantifies the polarisation of a dielectric material in response to an external electric field. We depict the temperature dependence of the susceptibility in Fig. 1.16. We observe a divergence of the susceptibility at $T = T_\mathrm{c}$, a hallmark of second order phase transitions. This divergence indicates that near a phase transition the material can very easily polarise even with a very small external field.

Overall, Landau theory in Eq. (1.18) provides a simple framework based on a quartic expression for the free energy from which we can qualitatively describe most features observed experimentally in second order phase transitions of many paraelectric-to-ferroelectric transitions. Notably, these include the vanishing of the polarisation and the divergence of the electric susceptibility at the transition temperature T_c. A simple extension of Eq. (1.18) to include a sixth order term also provides a simple framework to describe first order phase transitions, such as the paraelectric-to-ferroelectric phase transition in $BaTiO_3$.

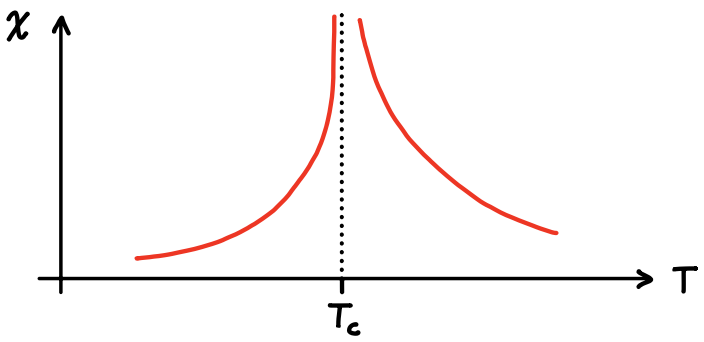

Figure 1.16: Schematic of the electric susceptibility as a function of temperature.

1.3.3 Polarisation domains

In the previous sections we have discussed structural phase transitions that drive a material from a non-polar to a polar phase. The discussion has focused on the unit cell, and the implicit assumption is that all unit cells in the material behave in the same way due to translational symmetry. However, in real polar materials the polarisation is not uniform across the material, and in this section we discuss the concept of polarisation domains.

Consider two electric dipoles pointing in the same direction with interaction energy $U_{\uparrow\uparrow}$, and two electric dipoles pointing in opposite directions with interaction energy $U_{\uparrow\downarrow}$. In polar materials, $U_{\uparrow\uparrow} < U_{\uparrow\downarrow}$ so that the system minimises its energy when dipoles point in the same direction. This implies that in polar materials electric dipoles tend to align in the same direction, and we define a *polarisation domain* as a region in a material in which all dipoles point in the same direction.

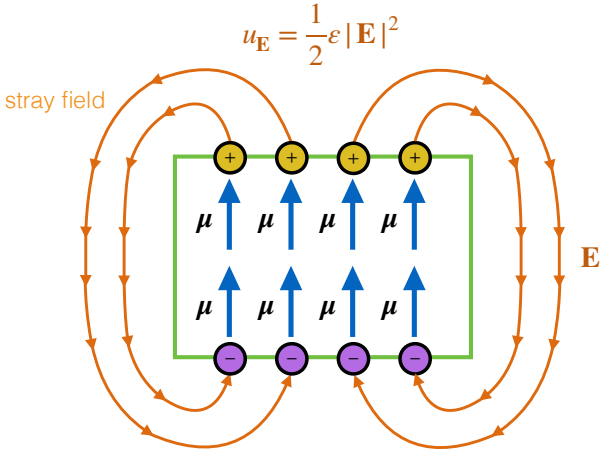

Figure 1.17: Schematic of stray field arising from monodomain material.

If the only relevant energy scale was that of dipole-dipole interactions, then all polar materials would have a single domain as all dipoles would align across the entire material. However, positive and negative charges would accumulate at opposite surfaces of such a monodomain material, and these charges would generate an electric field outside the material whose field lines would go from the positively charged surface to the negatively charged surface (see Fig. 1.17). Such an electric field is called a *stray field* whose energy density is:

$$u_{\mathbf{E}} = \frac{1}{2}\varepsilon|\mathbf{E}|^2. \tag{1.22}$$

This implies that there is an energy cost for a material to be in a monodomain configuration.

Overall, in polar materials there is a competition between the dipole-dipole interaction energy, which favours electric dipole alignment and large polarisation domains, against the stray field energy, which favours smaller domains to minimise surface charges. In real polar materials, the balance between these two energies leads to the appearance of multiple domains, separated by *domain walls* across which the polarisation changes direction. Figure 1.18 depicts two common examples of domains and domain walls.

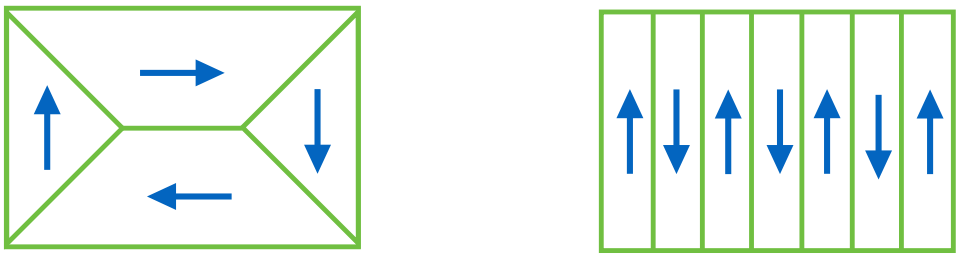

Figure 1.18: Schematic of domains in real polar materials. The diagram on the left depicts domains separated by 90° domain walls and the diagram on the right depicts domains separated by 180° domain walls.

The formation of domains and domains walls is a complex phenomenon that goes beyond the simple energy arguments discussed above. For example, their shape varies from material to material depending on features such as the underlying crystal symmetry. One reason for this is the coupling of polarisation to strain (piezoelectricity) which forces the domains to be compatible with the resulting strain fields in the material.

1.3.4 Hysteresis

If the polarisation direction in a polar material can be changed by the application of an external electric field, then the material is ferroelectric. In this section, we discuss how this reversal of polarisation occurs in real ferroelectric materials.

We can characterise the switch in polarisation direction in a ferroelectric by considering the dependence of the polarisation $\mathbf{P}$ on the applied electric field $\mathbf{E}$. The resulting curve is shown schematically in Fig. 1.19, and we discuss it in some detail next.

We start with an unpolarised sample ($\mathbf{P} = \mathbf{0}$) without an externally applied field ($\mathbf{E} = \mathbf{0}$), which is made of different domains pointing in different directions (Point 1 in Fig. 1.19). Upon the application of a small electric field, the polarisation of the material increases linearly with the applied field (standard dielectric response). This occurs through the growth of polarisation domains aligned with the applied field at the expense of other domains, and is mediated by the motion of domain walls. This process is fully reversible if the field is removed.

With increasing electric field strength, the aligned domains continue to grow at the expense of other domains and the polarisation undergoes a rapid increase (Point 2 in Fig. 1.19). This second regime is irreversible as the domain wall motion is pinned by defects in the material, a process that cannot be undone by simply removing the applied field.

Further increasing the electric field strength leads to a further increase in the polarisation, driven by the sweeping of the aligned domains through the material. The polarisation increase eventually saturates when the entire material is in a monodomain configuration (Point 3 in Fig. 1.19), and the resulting polarisation is called the *saturation polarisation* $\mathbf{P}_{\text{saturation}}$.

Once the system is fully polarised, the polarisation remains even with the removal of the external electric field. However, at zero external field the polarisation decresases slightly from the saturation value because when an electric field is present the system experiences a stronger

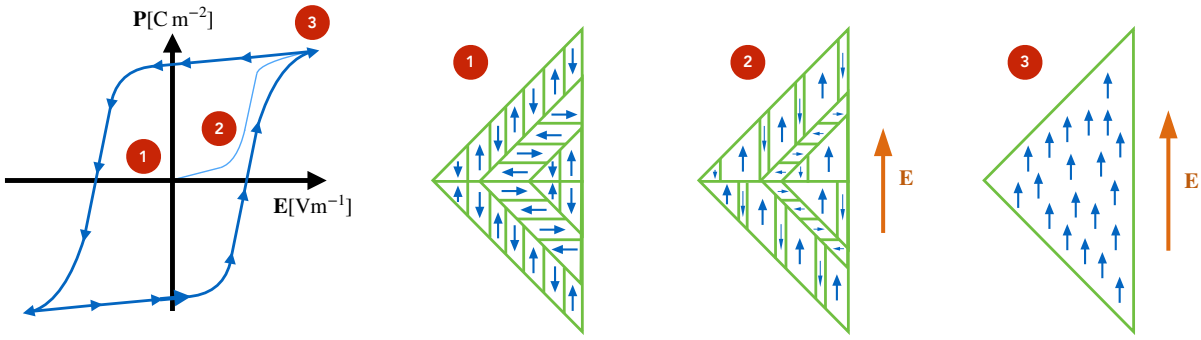

Figure 1.19: Hysteresis loop for the switching of a ferroelectric with the domain structure highlighted at three points along the path.

polarisation, for example due to a larger distortion of electron clouds. The resulting polarisation at zero field is called the *remanent polarisation* $\mathbf{P}_{\text{remanent}}$.

At this point, it is possible to decrease and eventually reverse the polarisation direction by applying a reverse external electric field in the opposite direction. Upon the application of such a field, small domains along the applied field (and opposite to the polarisation of the sample) start appearing. Increasing the reverse field eventually drives the sample into a depolarised state, in which domains of both orientations coexist. The field required to depolarise an initially polarised sample is called the *coercive field* $\mathbf{E}_{\text{coercive}}$.

Further increasing the reverse electric field drives the growth of domains aligned with it, such that the systems eventually becomes fully polarised again, but in the opposite direction. A saturation polarisation of the same magnitude but opposite direction to the original one is reached. At this point, the field can be again removed and reversed, and the system first depolarises and then polarises again in the original direction.

Overall, the cycle described above leads to the characteristic **E**–**P** *hysteresis loop* for the polarisation reversal of a ferroelectric material shown in Fig. 1.19. Microstructure engineering provides some control over the shape of a hysteresis loop. For example, increasing grain boundary concentration causes stronger domain wall pinning which leads to larger remanent polarisation and coercive field values.

1.3.5 Applications of ferroelectric materials

Ferroelectric materials find multiple technological applications. Many of these applications are based on the fact that ferroelectrics are dielectric materials with very high dielectric constants, for example the dielectric constant of $BaTiO_3$ is in the range $\kappa \sim 1{,}200$–$10{,}000$. High dielectric constants mean that ferroelectrics can, for example, be used to build capacitors that can store a lot of energy, and these are used in devices such as camera flashes.

Another prominent application of ferroelectric materials is in memory devices, which make direct use of their switchable polarisation. The basic principle is that opposite polarisation states of a ferroelectric material can be used to encode the values "0" and "1". In this context, writing to memory requires the switching of polarisation by the application of an external electric field. This process occurs through domain nucleation and growth and has a timescale of about 50 ns. Reading from memory can be accomplished by applying a field along the 0 direction, and if nothing happens then the reading is "0" while if a small current is detected (driven by the switch in polarisation) then the reading is "1". In the latter instance the polarisation needs to be reversed back to 1 after reading. Different materials can be used for memory applications of ferroelectrics, highlighting thin films of $LiNbO_3$, $PbTiO_3$, $Pb(Zr_xTi_{1-x})O_3$, and $SrBi_2Ta_2O_9$. Most modern memories are flash memories, which is an alternative technology that does not use ferroelectrics. However, ferroelectric memories do find niche applications such as in satellites

due to their radiation resistance.

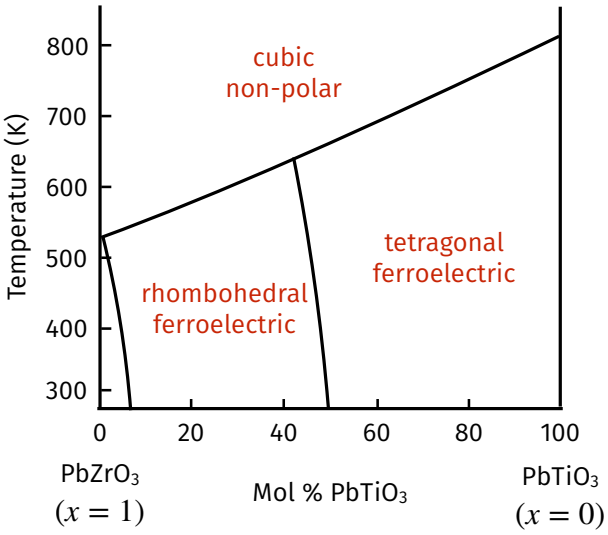

Figure 1.20: Schematic phase diagram of $Pb(Zr_xTi_{1-x})O_3$.

The use of ferroelectric materials in technological devices often requires the optimisation of their properties. For example, memory devices require ferroelectrics with high remanent polarisation (so that it is easy to measure) and small coercive fields (to minimise energy required for switching). In this context, a commonly used material in many applications of ferroelectrics is $Pb(Zr_xTi_{1-x})O_3$, also known as PZT, whose schematic phase diagram is shown in Fig. 1.20. At a concentration of about $x = 0.5$, PZT exhibits a phase transition between rhombohedral and tetragonal ferroelectric phases. The rhombohedral phase has 8 possible polarisation directions, while the tetragonal phase has 6 possible polarisation directions. Combined, PZT near the phase boundary is an extremely versatile material that can be polarised in many directions, making it extremely useful in technological applications.

Chapter 2

Magnetic materials

Maxwell's theory of electromagnetism provides a unifying framework for the phenomena of electricity and magnetism. In materials, it is often the case that one or the other dominates, and we have discussed the important role of electric fields in dielectric materials in the previous Chapter. In this Chapter, we focus on the interplay between magnetism and materials by exploring the basic classes of magnetic materials and their properties.

2.1 Microscopic origin of magnetism

Humans have known about magnetism for thousands of years. It was initially discovered in lodestones, naturally magnetised pieces of the mineral magnetite, and early applications included the navigational compass. Despite this long history, a fundamental understanding of magnetic materials only became possible over the past century with the parallel developments of Maxwell's theory of electromagnetism and quantum mechanics. In this Section, we introduce some key aspects of the microscopic origin of magnetism.

2.1.1 Magnetic moment

From electromagnetism theory, the relationship between electric currents I and magnetic fields $\mathbf{H}$ is described by Ampère's law:

$$\oint_P \mathbf{H} \cdot d\mathbf{l} = I. \tag{2.1}$$

This equation states that the circulation of a magnetic field $\mathbf{H}$ around a closed path P (left hand side) is equal to the total current I enclosed by the path (right hand side). The vector element $d\mathbf{l}$ is parallel to the path at every point along P. Qualitatively, Ampère's law states that electric currents generate magnetic fields, and an example is illustrated in Fig. 2.1 for a straight line current.

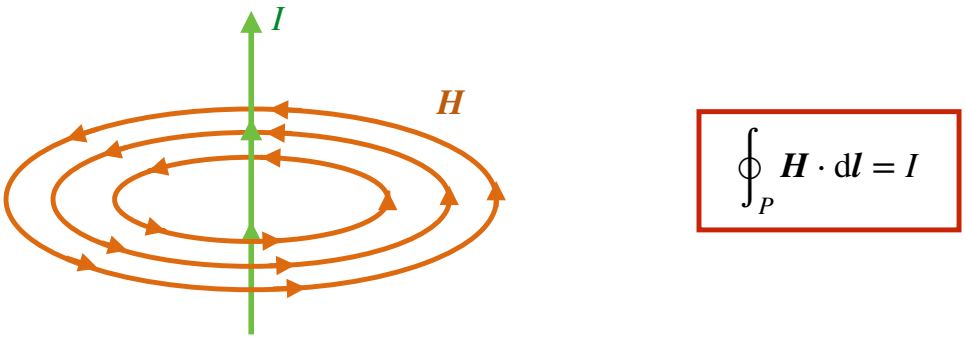

Figure 2.1: Illustrations of Ampère's law for a straight line current.

The magnetic field generated by a current depends on the magnitude and shape of the current. A straight line current generates a magnetic field consisting of concentric magnetic field circles (Fig. 2.1). Instead, a loop current generates the magnetic field depicted in the left diagram of Fig. 2.2.

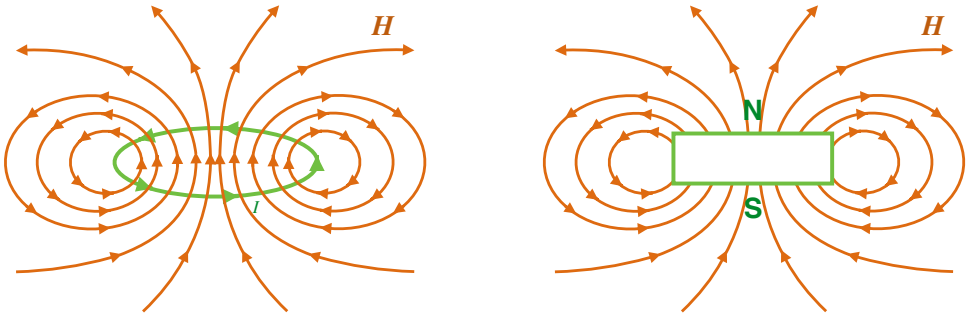

Figure 2.2: Magnetic field generated by a current loop (left) and by a bar magnet (right).

The magnetic field generated by a small current loop is identical to that generated by a magnet, as depicted in Fig. 2.2. In this context, *small* means that the loop is small compared to the distance at which the magnetic field is observed. Based on this observation, Ampère hypothesised that magnetic effects in materials such as iron were due to "molecular currents", a remarkable statement given that it was made 100 years before the discovery of the electron. Indeed, we now know that magnetic effects in materials are caused by the orbital and spin angular momenta associated with electrons (see further details in Appendix B).

Figure 2.3: Magnetic moment characterising a current loop.

Irrespective of its microscopic origin, we define a *magnetic moment* $\mathbf{m}$ as a vector quantity that characterises the strength and direction of *something* (e.g. a loop current or a bar magnet) that generates a magnetic field. For example, for a current I around a loop enclosing a circular area a, the magnetic moment has magnitude:

$$m = Ia, \tag{2.2}$$

and direction as depicted in Fig. 2.3. The magnetic moment has units of $[\mathrm{Am}^{-2}]$. Specifically, the magnetic moment is defined in the limit of the loop of current becoming very small while keeping m fixed, so that as a decreases I must increase. Analogously, the magnetic moment for a bar magnet is defined in the limit of the magnet becoming very small.

2.1.2 Magnetisation and susceptibility

In a material, we define the *magnetisation* as the density of magnetic moments. Mathematically, the magnetisation $\mathbf{M}$ is given by:

$$\mathbf{M} = n\mathbf{m}, \tag{2.3}$$

where n is the number of magnetic moments per unit volume with units $[\mathrm{m}^{-3}]$. The magnetisation is a vector quantity of units $[\mathrm{Am}^{-1}]$. The magnetisation in magnetic materials is analogous to the polarisation in dielectric materials.

We characterise the magnetisation $\mathbf{M}$ induced by an external magnetic field $\mathbf{H}$ in a material through the *magnetic susceptibility* χ, which is defined through the equation:

$$\mathbf{M} = \chi \mathbf{H}. \tag{2.4}$$

Qualitatively, a material with a large susceptibitily can be more readily magnetised by an external magnetic field compared to a material with a low susceptibility. Additionally, a positive susceptibility $\chi > 0$ indicates that the magnetic moments in a material align with the applied field and a negative susceptibility $\chi < 0$ indicates that the magnetic moments in a material align against the applied field.

2.2 Classification of magnetic materials

Magnetic materials can be classified into different classes depending on their magnetisation and susceptibility, with a schematic summary of the classification shown in Fig. 2.4.

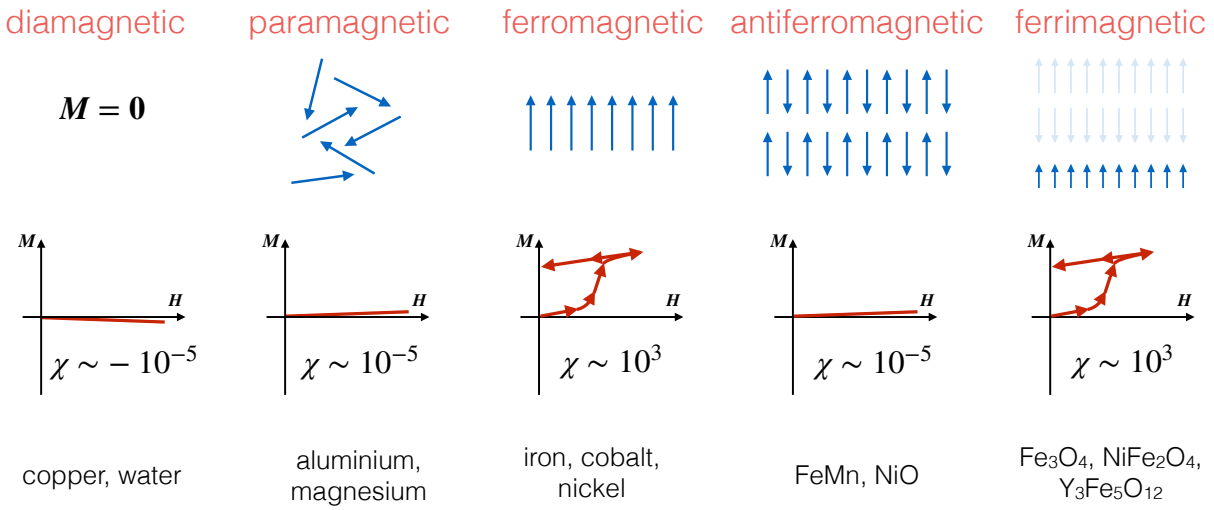

Figure 2.4: Classification of magnetic materials according to their magnetisation and susceptibility.

2.2.1 Diamagnetic materials

From electromagnetism theory, the currents induced by a magnetic field can be characterised with Lenz's law:

$$\mathcal{E} = -\frac{d\Phi_{\mathbf{B}}}{dt}. \tag{2.5}$$

Qualitatively, this equation states that an electromotive force $\mathcal{E}$ is generated in a loop of wire by the rate of change of magnetic flux $\Phi_{\mathbf{B}}$ through that loop. Crucially, the negative sign means that the currents induced by a magnetic field act to oppose the applied magnetic field.

In this context, *diamagnetism* refers to the change in orbital motion of electrons in opposition to an applied magnetic field. All atoms are diamagnetic, but diamagnetism is a relatively weak phenomenon so in most materials it is masked by other magnetic interactions which are stronger. *Diamagnetic materials* are materials in which diamagnetism is the only magnetic phenomenon.

Diamagnetic materials are characterised by a vanishing magnetisation $\mathbf{M} = \mathbf{0}$ and a small negative susceptibility $\chi \sim -10^{-5}$. The negative susceptibility is a reflection of Lenz's law whereby the orbital motion of electrons is such as to oppose the applied magnetic field. This implies that diamagnetic materials are repulsed by magnetic fields, which leads to striking phenomena such as magnetic levitation.

Examples of diamagnetic materials include copper and water.

2.2.2 Paramagnetic materials

We can associate magnetic moments with atoms having partially filled atomic shells. When the interactions between these magnetic moments are weak compared to other energy scales (e.g. thermal energy), the magnetic moments orient in random directions and the overall magnetisation of the material vanishes, $\mathbf{M} = \mathbf{0}$. Upon the application of an external magnetic field, magnetic moments weakly align with it (see Fig. 2.5). This leads to a small magnetisation that can be characterised by a small positive susceptibility $\chi \sim 10^{-5}$. Materials that behave in this manner are called *paramagnetic materials*. Examples of paramagnetic materials include aluminium and magnesium.

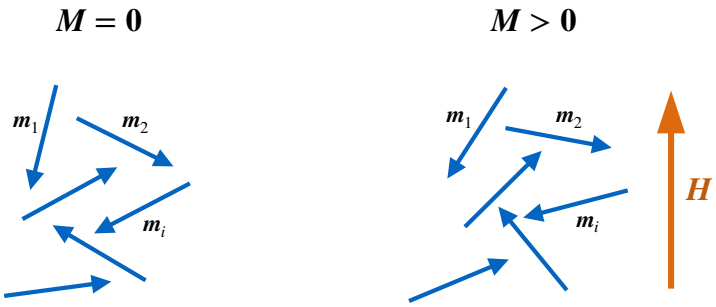

Figure 2.5: Magnetic moments in a paramagnetic material without an external field (left) and in the presence of an external field (right).

2.2.3 Ferromagnetic materials

A *ferromagnetic material* is a material in which the magnetic moments associated with atoms interact strongly and this interaction favours aligned moments. This leads to a large and positive magnetisation $\mathbf{M} > \mathbf{0}$ and to a positive and large magnetic susceptibility $\chi \sim 10^3$. Examples of ferromagnetic materials include iron, cobalt, and nickel.

We discuss ferromagnetic materials in detail in Sec. 2.3 below.

2.2.4 Antiferromagnetic materials

An *antiferromagnetic material* is a material in which the magnetic moments associated with atoms interact strongly and this interaction favours antialigned moments. This leads to a vanishing magnetisation $\mathbf{M} = \mathbf{0}$ and to a positive and small magnetic susceptibility $\chi \sim 10^{-5}$. Note that a key difference between paramagnetic and antiferromagnetic materials is that the magnetic moments are randomly oriented in the former but ordered in an antialigned fashion in the latter (see Fig. 2.4).

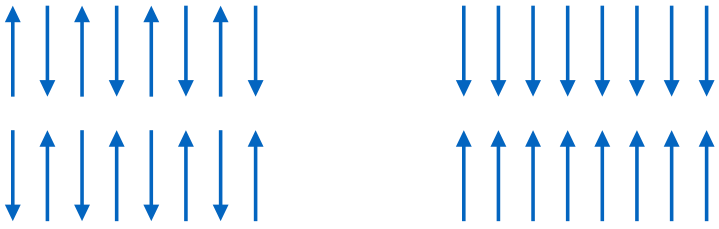

Figure 2.6: Examples of magnetic moment ordering in antiferromagnetic materials.

Antiferromagnetic materials can exhibit complex ordering of magnetic moments. In some systems, the interaction between magnetic moments can favour alignment between some moments and antialignment between others, but as long as the net magnetisation vanishes, we still

have an antiferromagnetic material. Two different examples of antiferromagnetic alignment are shown in Fig. 2.6. In the left diagram, every single moment is antialigned with all its neighbours; in the right diagram, magnetic moments are ferromagnetically aligned within horizontal planes, but antiferromagnetically aligned between planes, leading to an overall zero magnetisation.

Examples of antiferromagnetic materials include ferro manganese (FeMn) and nickel oxide (NiO).

2.2.5 Ferrimagnetic materials

A *ferrimagnetic material* is a material in which atoms with opposing magnetic moments exist, as in antiferromagnetic materials, but the magnitudes of the moments are different resulting in a non-vanishing magnetization $\mathbf{M} \neq \mathbf{0}$. As a result of the non-zero magnetisation, even in the absence of an applied field, their susceptibility behaves in a similar manner to that of ferromagnetic materials. Examples of ferrimagnetic materials include magnetite (Fe_3O_4), nickel ferrite ($NiFe_2O_4$), and yttrium iron garnet ($Y_3Fe_5O_{12}$).

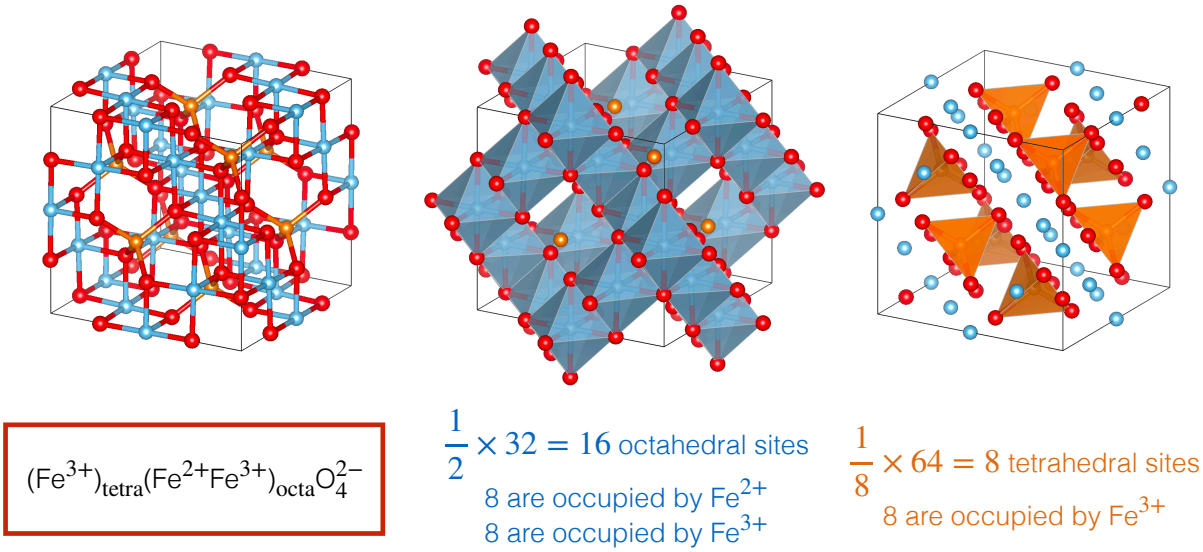

Figure 2.7: Crystal structure of magnetite (left), highlighting the octahedral sites (centre) and the tetrahedral sites (right).

To illustrate magnetic ordering in a ferrimagnetic material, we consider the structure of magnetite, which adopts an inverse spinel structure as shown in Fig. 2.7. In this structure, the oxygen atoms are arranged in a face-centred cubic (fcc) sublattice, and the primitive cell of magnetite is composed of a supercell of size $2 \times 2 \times 2$ of the conventional fcc cubic cell. We can identify two types of interstices in a fcc lattice, octahedral interstices and tetrahedral interstices, as depicted in Fig. 2.8 for a conventional fcc unit cell. In such a conventional fcc unit cell, there are four octahedral sites and eight tetrahedral sites, which become 32 octahedral sites and 64 tetrahedral sites for the $2 \times 2 \times 2$ oxygen sublattice supercell that makes up the magnetite primitive cell.

The iron atoms in magnetite occupy both octahedral and tetrahedral sites: they occupy 16 of the 32 octahedral sites and 8 of the 64 tetrahedral sites. Additionally, iron atoms in magnetite occur in two different oxidation states, Fe^{2+} and Fe^{3+}. All Fe^{2+} ions occupy octahedral sites (8 out of 16 occupied sites), while Fe^{3+} ions occupy the remaining 8 octahedral sites and all 8 tetrahedral sites. Overall, there are 8 Fe^{2+} ions and 16 Fe^{3+} ions in a primitive cell of magnetite. The iron sites and oxidation states are schematically shown in Fig. 2.7.

In magnetite, the magnetic moments of Fe^{3+} ions in octahedral and tetrahedral sites point in opposite directions, and their overall contribution to the magnetisation vanishes. The magnetic

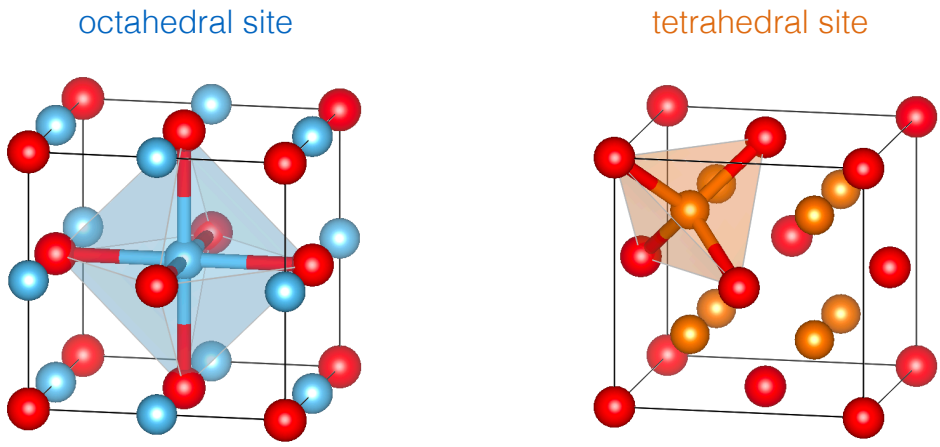

Figure 2.8: Conventional fcc unit cell of red oxygen atoms with blue octahedral interstice sites (left) and orange tetrahedral interstice sites (right).

moments associated with Fe^{2+} ions in the octahedral sites all align with each other, and have no counter-balancing moments. As a result, magnetite has a non-zero magnetisation and is a ferrimagnetic material.

2.3 Ferromagnetism

Like ferroelectrics, ferromagnets play a key role in both fundamental and applied science. In this Section, we discuss some key ideas associated with ferromagnetism, drawing some parallels with ferroelectricity while also highlighting key differences.

2.3.1 Exchange interaction

Ferromagnetic materials have atomic magnetic moments that interact strongly and this interaction favours aligned moments. The microscopic origin of this interaction is quantum mechanical in nature, and is a consequence of the *exchange interaction* between electrons.

The Pauli exclusion principle states that no two electrons can occupy the same quantum state, and is a manifestation of a fundamental property of identical quantum particles that is called the exchange interaction [1]. Electron states in quantum mechanics are described by a mathematical object called the *wave function*. This wave function has two parts: a spatial part and a spin part. The spatial part is associated with the distribution of electrons in space and the spin part is associated with the spin angular momentum of electrons and can take one of two possible values. In this context, the Pauli exclusion principle implies that no two electrons can simultaneously have the same spatial *and* spin parts of their wave functions.

If we consider two electrons, they can have the same spatial part of the wave function as long as their spins are opposite. When two electrons have the same spatial part of the wave function, they experience a strong Coulomb repulsion because they are negatively charged. By contrast, if two electrons have the same spin, they must have different spatial wave functions to obey the Pauli exclusion principle. In this case, their spatial overlap is small leading to a weak Coulomb repulsion. The latter case leads to a lower energy configuration, which implies that the exchange interaction favours parallel spins. It is this alignment of spins that manifests itself as the alignment of magnetic moments in ferromagnetic materials.

In ferromagnetic materials there is a competition between the exchange interaction, which favours magnetic moment alignment, and thermal energy, which randomises the order of mag-

[1] The Pauli exclusion principle has profound implications, including the shell structure of atoms and the stability of white dwarf stars and neutron stars.

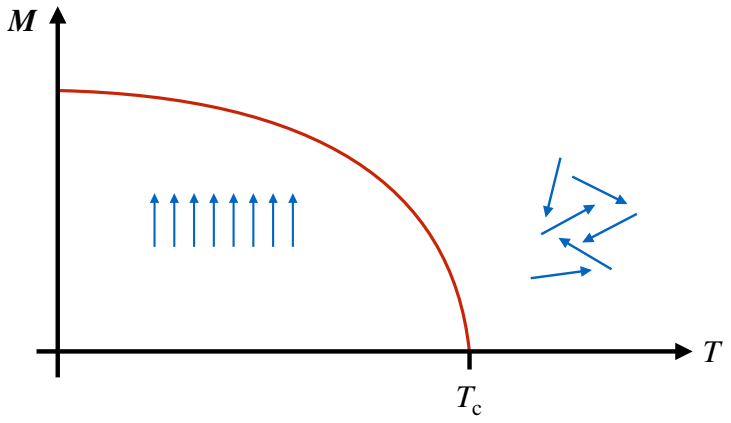

Figure 2.9: Schematic phase diagram of the magnetisation as a function of temperature for a ferromagnetic material.

netic moments. As a result of this competition, ferromagnetic materials exhibit a larger magnetisation at low temperatures, which decreases with increasing temperature. Beyond some critical temperature, called the *Curie temperature* T_c, magnetic moments become fully random, so that the magnetisation disappears and the material undergoes a ferromagnetic-to-paramagnetic phase transition. The magnetisation-temperature phase diagram of a ferromagnetic system is schematically depicted in Fig. 2.9.

The ferromagnetic-paramagnetic phase transition is similar to the ferroelectric-paraelectric phase transition discussed in Sec. 1.3. A key difference is that the ferroelectric-to-paraelectric transition is driven by structural changes associated with inversion symmetry. In ferromagnets, there is no need for a structural phase transitions as spins are mostly free to align in any direction irrespective of the underlying crystal structure (although see discussion on magnetocrystalline anisotropy in Sec. 2.3.2 below).

2.3.2 Anisotropy

Anisotropy refers to the dependence of the properties of a material on direction. Anisotropy plays an important role in ferromagnetic materials, and in this section we describe some of its manifestations.

Ferromagnetic materials exhibit *magnetocrystalline anisotropy*. This anisotropy is caused by the interaction of magnetic moments with the underlying crystal lattice, and has its origins in a quantum mechanical and relativistic phenomenon called the spin-orbit interaction. As a result of magnetocrystalline anisotropy, ferromagnetic materials have an *easy axis* along which the application of a magnetic field leads to a rapid increase of the magnetisation, which saturates at relatively low fields. By contrast, applying the same magnetic field along a *hard axis* leads to a more gradualy increase of the magnetisation, which only saturates at relatively higher fields. The response of a ferromagnetic material along easy and hard axes is schematically shown in Fig. 2.10.

Different materials have different easy axes. For example, α-iron, a ferromagnetic form of iron ($T_c = 771\,^\circ\mathrm{C}$) which adopts the body-centred cubic (bcc) structure, has easy axes along the $\langle 100 \rangle$ cubic side directions and hard axes along the $\langle 111 \rangle$ body diagonal directions. By contrast, face-centred cubic (fcc) nickel has the easy axes along the $\langle 111 \rangle$ directions and the hard axes along the $\langle 100 \rangle$ directions.

Ferromagnetic materials also exhibit *shape anisotropy*. Consider a ferromagnetic bar with the traditionally called "north" and "south" poles. Field lines outside the bar magnet go from north to south (orange field lines in Fig. 2.11). There is also a *demagnetising field* inside the bar magnet that acts against the magnetisation that creates the north and south poles in the

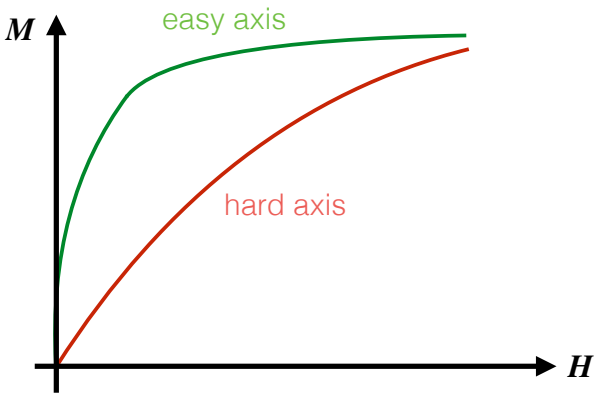

Figure 2.10: Schematic of the magnetisation as a function of applied magnetic field along the easy and hard axes.

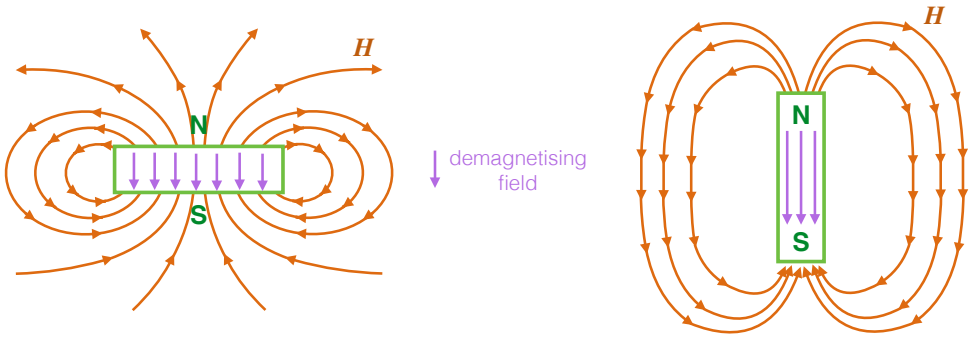

Figure 2.11: Generated field (orange) and demagnetising field (purple) for two bar magnets.

first place (purple field lines in Fig. 2.11). This demagnetising field depends on the shape of the sample, but if we focus on elongated samples such as those depicted in Fig. 2.11, then the demagnetising field is largest along the short axis and smallest along the long axis. This implies that it is easier to build a bar magnet with the north and south poles at the thin ends of the sample (right hand side of Fig. 2.11) compared to the thick ends (left hand side of Fig. 2.11).

Ferromagnetic materials also exhibit a related phenomenon, called *magnetostriction*, which is a change in shape when the material is magnetised. The precise form that magnetostriction takes is material dependent; for example, bcc iron elongates along the easy direction of magnetisation, while fcc nickel contracts along its easy direction of magnetisation.

2.3.3 Domains and domain walls

Similar to ferroelectric materials, ferromagnetic materials are subject to an energy competition between the magnetic moment interaction that favours alignment between moments and the stray fields that favour small regions of aligned moments. As a result, ferromagnetic materials form magnetisation domains separated by domain walls.

The size of domain walls in ferromagnetic materials depends on the relative energies arising from the exchange interaction and magnetocrystalline anisotropy. The exchange interaction favours aligned magnetic moments (see Sec. 2.3.1), which leads to wide domain walls in which the moments change direction gradually in such a way as to maintain high alignment with all neighbours (see top diagram in Fig. 2.12). Magnetocrystalline anisotropy favours the alignment of magnetic moments along specific crystallographic directions, which leads to narrow domain walls in which moments change direction abruptly to maintain alignment along preferred crystallographic directions (see bottom diagram in Fig. 2.12). The overall nature of domain walls depends

on the relative importance of the exchange interaction and magnetocrystalline anisotropy in any given material.

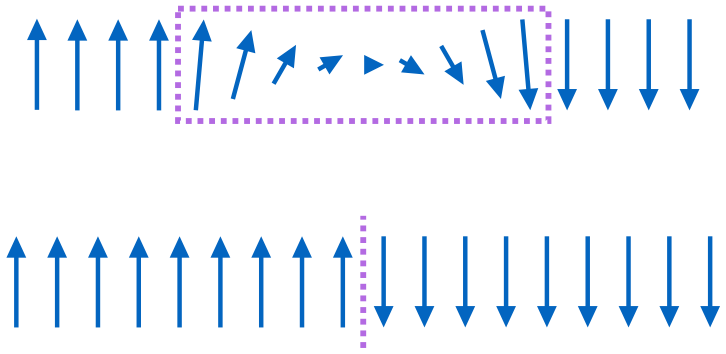

Figure 2.12: Schematic diagrams depicting wide (top) and narrow (bottom) magnetic domain walls.

Ferroelectric materials also host domains separated by domain walls (see Sec. 1.3.3). By comparison, domain walls in ferroelectrics are significantly narrower compared to those of ferromagnets because polarisation is strongly constrained to point along the crystallographic polar axes.

2.3.4 Hysteresis

In this section, we discuss how the reversal of magnetisation direction occurs in real ferromagnetic materials. In analogy to the change in polarisation direction in ferroelectrics, a hysteresis loop appears, whose broad features resemble those of ferroelectrics, but there are some differences.

We can characterise the switch in magnetisation direction in a ferromagnet by considering the dependence of the magnetisation $\mathbf{M}$ on the applied magnetic field $\mathbf{H}$. The resulting curve is shown schematically in Fig. 2.13, and we discuss it in some detail next.

We start with an demagnetised sample ($\mathbf{M} = \mathbf{0}$) without an externally applied field ($\mathbf{H} = \mathbf{0}$), which is made of different domains pointing in different directions (Point 1 in Fig. 2.13). The magnetisation directions in the domains are initially aligned along easy axes of the material.

Upon the application of a small magnetic field, the magnetisation increases linearly with the applied field. This occurs through the growth of magnetisation domains aligned with the applied field at the expense of other domains, and is mediated by the motion of domain walls. This process is fully reversible if the field is removed.

With increasing magnetic field strength, the aligned domains continue to grow at the expense of other domains and the magnetisation undergoes a rapid increase (Point 2 in Fig. 2.13). This second regime is irreversible as the domain wall motion is pinned by defects in the material, a process that cannot be undone by simply removing the applied field. Note that the magnetisation largely points along easy axes, even if the applied field is not exactly parallel to an easy axis. The domains that grow are those that are most aligned (but perhaps not perfectly aligned) with the applied field.

Further increasing the magnetic field strength leads to a further increase in the magnetisation, driven by the sweeping of the aligned domains through the material and resulting in a monodomain. Note that at this stage the magnetisation still points along the easy axis that is most aligned (but not necessarily perfectly aligned) with the applied field (Point 3 in Fig. 2.13). Increasing the magnetic field strength further eventually leads to a rotation of the magnetisation direction away from an easy axis to point exactly parallel with the applied field (Point 4 in Fig. 2.13). The resulting magnetisation is called the saturation magnetisation $\mathbf{M}_{\text{saturation}}$. Note that this last step in the magnetisation of a ferromagnet differs from the analogous process in the polarisation of a ferroelectric, because in a ferroelectric the polarisation is constrained along

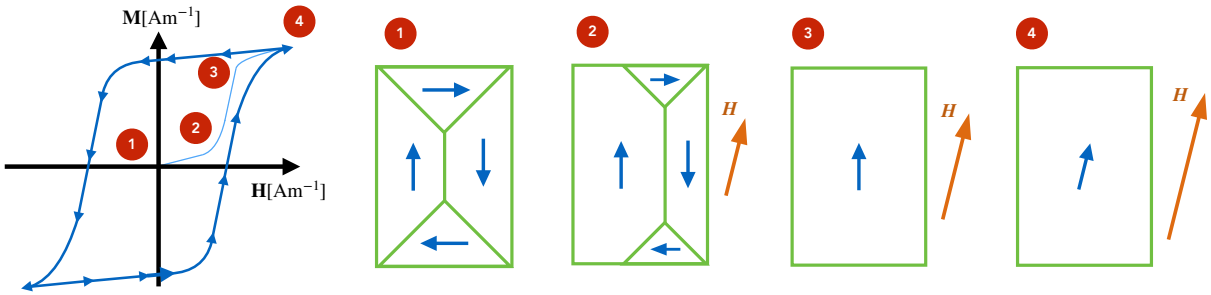

Figure 2.13: Generated field (orange) and demagnetising field (purple) for two bar magnets.

polar crystallographic directions and if these do not perfectly align with the applied electric field, then the polarisation in the fully polarised material never fully aligns with the applied field.

Once the system is fully magnetised, the magnetisation remains even with the removal of the external magnetic field. However, at zero external field the magnetisation decresases slightly from the saturation value because some small domains in the opposite direction start nucleating due to the demagnetisation field in the sample. Additionally, the magnetisation direction rotates back to point along an easy axis when the external field is removed.

At this point, it is possible to decrease and eventually reverse the magnetisation direction by applying a reverse external magnetic field in the opposite direction. Upon the application of such a field, small domains along the applied field (and opposite to the magnetisation of the sample) start growing. Increasing the reverse field eventually drives the sample into a demagnetised state, in which domains of both orientations coexist. The field required to demagnetise an initially magnetised sample is called the coercive field $\mathbf{H}_{\text{coercive}}$.

Further increasing the reverse magnetic field drives the growth of domains aligned with it, such that the systems eventually becomes fully magnetised again, but in the opposite direction. A saturation magnetisation of the same magnitude but opposite direction to the original one is reached. At this point, the field can be again removed and reversed, and the system first demagnetises and then magnetises again in the original direction.

Overall, the cycle described above leads to the characteristic **M**–**H** hysteresis loop for the magnetisation reversal of a ferromagnetic material shown in Fig. 2.13.

2.3.5 Applications of ferromagnetic materials

Ferromagnetic materials find multiple technological applications. One prominent example is the use of soft ferromagnets in transformers. A transformer is a device that transfers energy between electrical circuits by exploiting a varying current in one circuit that produces a varying magnetic flux that in turn drives a varying electromotive force that can drive a current in a separate circuit. For transformer applications we need magnets whose magnetisation direction can be easily switched, and this requires high purity samples in which domain walls can easily travel through the sample to drive magnetisation and demagnetisation.

Another application is that of permanent magnets, which use hard ferromagnetic materials. In these, the requirements are large coercive fields and high zero-field magnetisation, which require microstructure with defects that can pin the motion of domain walls.

Chapter 3

Ionic conductors

The ability of a material to conduct electricity is characterised by its *conductivity* σ, with units of siemens per metre [Sm^{-1}]. Alternatively, one can use the reciprocal quantity, called the *resistivity* ρ, with units of ohm-metre [Ωm].

Metals are materials with high conductivities mediated by the motion of negatively charged electrons. For example, the conductivity of gold is $4.1 \times 10^7\,\mathrm{Sm}^{-1}$, the conductivity of silver is $6.3 \times 10^7\,\mathrm{Sm}^{-1}$, and the conductivity of copper is $6.0 \times 10^7\,\mathrm{Sm}^{-1}$. By contrast, electronic insulators are materials in which electrons are not free to move, and they have conductivities orders of magnitude smaller. For example, the conductivity of air is $5 \times 10^{-15}\,\mathrm{Sm}^{-1}$, the conductivity of glass is $10^{-13}\,\mathrm{Sm}^{-1}$, and the conductivity of aluminium oxide is $10^{-10}\,\mathrm{Sm}^{-1}$.

In this Chapter we study materials whose conductivities are intermediate to those of metals and insulators. In these materials, electrons are not free to move so cannot contribute to the conductivity, but ions can move and are the main contributors to the conductivity. For this reason, these materials are called *ionic conductors*. An example of an ionic conductor is yttria-stabilised zirconia, whose conductivity is about $0.1\,\mathrm{Sm}^{-1}$.

3.1 Ionic conductivity

The motion of microsopic charges plays a key role in many areas of science and technology. In this Section, we first describe the general phenomenology of charge transport, and then focus on its illustration in the case of ionic conduction.

3.1.1 Diffusion

From the theory of statistical mechanics, concentration gradients in microscopic particles lead to diffusion of particles to homogenise the concentration. The resulting *diffusion flux* J is defined as the number of particles crossing unit area in unit time:

$$J = \frac{I}{A}, \tag{3.1}$$

where I is the current of particles and A the area they cross. The units of diffusion flux J are [$\mathrm{m}^{-2}\mathrm{s}^{-1}$], the units of current I are [s^{-1}], and the units of area are [m^2]. In the most general situation, the diffusion flux is a vector quantity, but the key ideas we will discuss can be illustrated by only considering the scalar definition in Eq. (3.1), which implicity assumes that the current of particles is perpendicular to the area.

Mathematically, we quantify the relationship between concentration n and diffusion flux J through *Fick's first law of diffusion*, which in one dimension reads:

$$J_x = -D\frac{\partial n}{\partial x}. \tag{3.2}$$

In this equation, D is the diffusion coefficient (also called diffusivity) and has units of $[\mathrm{m^2 s^{-1}}]$. Note that we have a partial derivative with respect to position x because the concentration is in general a function of both space and time, $n(x,t)$. Qualitatively, Eq. (3.2) states that the diffusion flux is proportional to the concentration gradient, and the proportionality constant is the diffusivity. The minus sign in Eq. (3.2) indicates that the flux flows from higher to lower concentration regions.

Fick's first law involves the diffusion flux J for arbitrary particles. For charged particles, we can define the analogous current density j, which obeys the related equation:

$$j_x = -qD\frac{\partial n}{\partial x}, \tag{3.3}$$

where q is the charge of the particle. The units of j are $[\mathrm{Am^{-2}}]$.

For completeness, Fick's second law of diffusion relates the temporal and spatial variations in the concentration through:

$$\frac{\partial n}{\partial t} = D\frac{\partial^2 n}{\partial x^2}. \tag{3.4}$$

This equation is discussed in detail in Course D.

3.1.2 Drift

From electromagnetism theory, remember Ohm's law $I = \frac{V}{R}$, which relates the current I through a circuit element to the voltage drop V across that element, quantified by the resistance R. The microscopic version of Ohm's law reads:

$$\mathbf{j} = \sigma\mathbf{E}, \tag{3.5}$$

where $\mathbf{j}$ is the current density, σ is the conductivity, and $\mathbf{E}$ is the applied electric field. Further relating the electric field with the potential, $\mathbf{E} = -\nabla V$, we can re-write the microscopic version of Ohm's law as:

$$j_x = \sigma E_x = -\sigma\frac{\partial V}{\partial x}, \tag{3.6}$$

where we again limit our discussion to one dimension. Qualitatively, Eq. (3.6) describes the *drift current* that is driven by a potential difference (or equivalently by an applied electric field). An important subtlety is that the current density is defined as the motion of *positive charges*. If the moving particles are positively charged, then they flow from areas of high voltage to areas of low voltage and the current density points in the same direction. If the moving particles are negatively charged, then they flow from areas of low voltage to areas of high voltage, but the current density is still in the same direction as above as the motion of negative charges in one direction is equivalent to the motion of positive charges in the opposite direction.

3.1.3 Nernst-Einstein equation

In the presence of an applied electric field, we can generalise Eq. (3.3) to:

$$j_x = -qD\frac{\partial n}{\partial x} - \sigma\frac{\partial V}{\partial x}. \tag{3.7}$$

This equation states that the net current density is the combination of the diffusion current arising from concentration gradients and the drift current arising from an applied electric field.

A system with an initially arbitrary concentration profile and an applied field will experience a combination of diffusion and drift currents driving it towards a steady state in which the concentration profile does not change $\frac{\partial n}{\partial x} = 0$. In this steady state, there is no net current density $j_x = 0$, and Eq. (3.7) becomes:

$$-qD\frac{\partial n}{\partial x} - \sigma\frac{\partial V}{\partial x} = 0. \tag{3.8}$$

Assuming a Boltzmann distribution for the concentration of diffusing particles n in the presence of a potential V, namely $n = n_0 e^{-qV/k_\mathrm{B}T}$, we arrive at the *Nernst-Einstein equation*:

$$\frac{\sigma}{D} = \frac{nq^2}{k_\mathrm{B}T}, \tag{3.9}$$

where $k_\mathrm{B} = 1.380649 \times 10^{-23}\,\mathrm{JK}^{-1}$ is Boltzmann's constant and T is temperature. The derivation of Eq. (3.9) is detailed in Problem 9. Qualitatively, Eq. (3.9) relates the diffusion coefficient D and the conductivity σ of charged particles at the steady state to the concentration n, the charge q, and the temperature T.

3.1.4 Defects in materials

The discussion in the preceding sections concerns the general properties of the diffusion and drift of arbitrary charged particles subject to concentration gradients and applied electric fields. In this section, we make this discussion concrete by considering the example of ionic conductors, in which the microcopic particles are the ions in a material. Ionic conduction in materials is mediated by defects, so we next turn our attention to defects in materials.

All materials have defects, which can be zero-dimensional (point defects), one-dimensional (line defects), or two-dimensional (plane defects). Our focus is on point defects, which in turn come in many forms, for example:

- Vacancy defects: missing atoms.
- Interstitial defects: extra atoms in the crystal.
- Substitutional defect: replacing one atom by another atom.
- Antisite defect: exchanging the positions of two atoms.
- Topological defects: local changes in bonding.

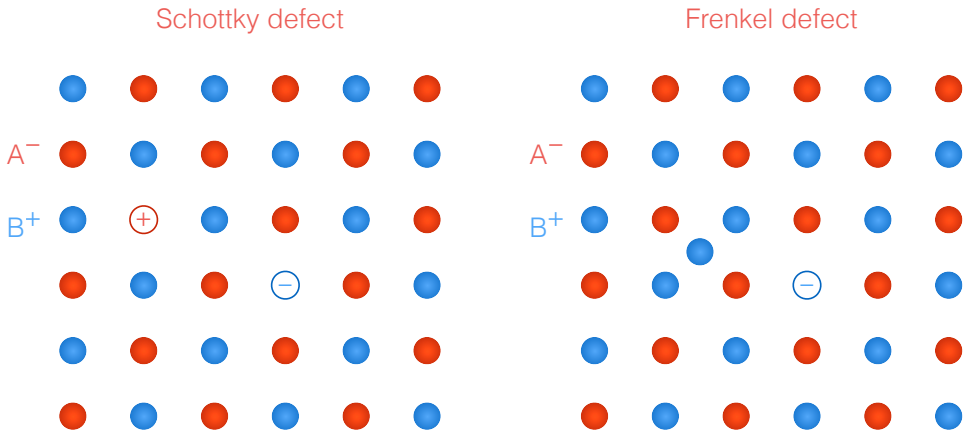

Figure 3.1: Schematic diagrams of stoichiometric Schottky (left) and Frenkel (right) defects in a simple $\mathrm{A}^-\mathrm{B}^+$ ionic compound.

Of particular interest to ionic diffusion are so-called stoichiometric defects that do not change the stoichiometry of the material. Of these, we have *Schottky defects*, in which two ions of opposite charge are missing simultaneously (left diagram in Fig. 3.1); and *Frenkel defects*, in which one vacancy forms at a lattice site with an interstitial of the same atom forming elsewhere (right diagram in Fig. 3.1). Note that we can assign a charge with a vacancy, which is the opposite to the charge of the ion that was occupying that site, and is represented by an open

circle in Fig. 3.1. Schottky defects occur in many ionic compounds, such as sodium chloride (NaCl) or cubic zirconia (ZrO_2). Frenkel defects also occur in many ionic compounds, such as zinc sulfide (ZnS) and silver chloride (AgCl), and these usually happen in compounds with small ions that can fit in interstitial sites.

3.1.5 Ionic motion in materials

Ionic motion in materials is mediated by defects such as Schottky defects. The key step is the motion of an ion from its original crystallographic site into a nearby vacant site, as schematically illustrated in Fig. 3.2. The original and final ionic positions correspond to low energy configurations, and they are separated by an energy barrier E_B. The magnitude of the energy barrier is material specific, and even within a single material also depends on the precise initial and final configurations.

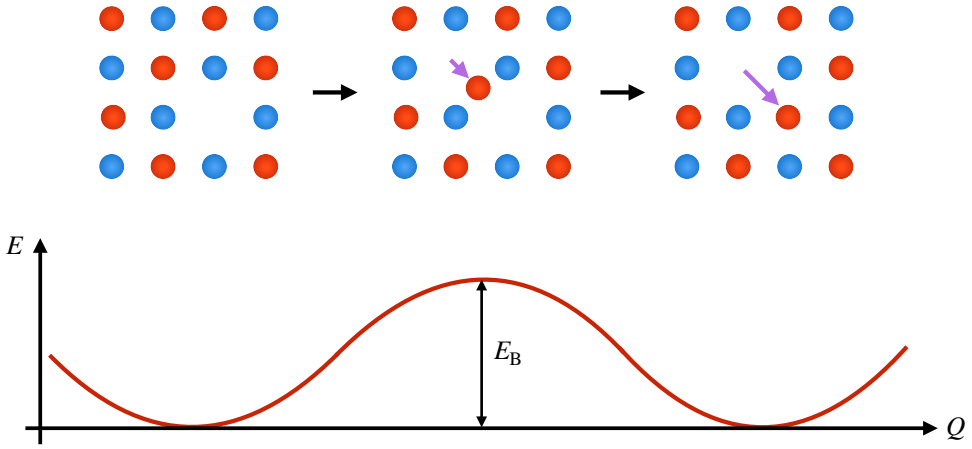

Figure 3.2: Schematic diagrams of an ionic jump from an initial site (left) through a saddle point (middle) into a vacant site (right). The energy profile of such a process is depicted in the bottom diagram, where Q refers to a generalised coordinate describing the atomic configurations along the transition.

How does an ion move from one site to another through the energy barrier E_B? This is an example of a thermally activated process, in which thermal energy drives the transition through the energy barrier. Similar physics occurs in a wide variety of contexts, for example in chemical reactions. Mathematically, this process is described by the *Arrhenius equation*, which gives the diffusivity D as a function of the energy barrier and temperature according to:

$$D = D_0 e^{-\frac{E_\mathrm{B}}{k_\mathrm{B}T}}. \tag{3.10}$$

The pre-exponential factor D_0, which has units of diffusivity [$\mathrm{m^2 s^{-1}}$], depends on the jump distance (e.g. the lattice constant in a simple cubic structure) and the jump attempt rate, which is related to the oscillation frequency of the atoms.

In the limit of a small applied electric field, such that $qV \ll k_\mathrm{B}T$, the following Arrhenius relation holds:

$$\ln\sigma = \ln\sigma_0 - \left(\frac{E_\mathrm{B}}{k_\mathrm{B}}\right)\frac{1}{T}, \tag{3.11}$$

where $\sigma_0 = \frac{D_0 n_0 q^2}{k_\mathrm{B}T}$, and n_0 is the zero-temperature concentration of ions. The derivation of Eq. (3.11) is detailed in Problem 12.

As $\ln(\frac{1}{T})$ varies much more slowly than $\frac{1}{T}$, we can take $\ln\sigma_0$ to be approximately constant. In this approximation, the Arrhenius relation in Eq. (3.11) implies that a plot of the logarithm of the conductivity $\ln\sigma$ against $\frac{1}{T}$ will be an approximate straight line with slope $-\frac{E_\mathrm{B}}{k_\mathrm{B}}$ and intercept

$\ln \sigma_0$. In practice, such Arrhenius plots are used to characterise the microscopic properties of different ionic conductors, as exemplified in Fig. 3.3.

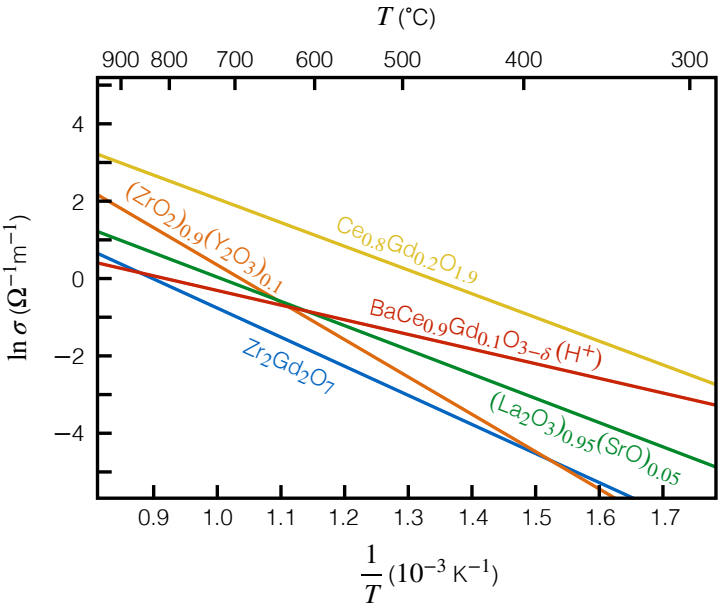

Figure 3.3: Arrhenius plot for representative ionic conductors.

Another important consequence of Eq. (3.11) is that conductivity σ increases with increasing temperature. This is a hallmark of ionic conductors, and its origin is the thermally-activated diffusivity that arises from the energy profile of the transition of ions between sites depicted in Fig.3.2. As a result, ionic conductors are typically used at relatively high temperatures to promote conductivity.

3.2 Ionic conducting materials

In this Section, we describe the structure of two ionic conductors: yttria-stabilised zirconia and bismuth oxide.

3.2.1 Yttria-stabilised zirconia

A prominent ionic conducting material is yttria-stabilised zirconia, in which the ionic conduction is mediated by O^{2-} ions. In this section, we introduce the structure of yttria-stabilised zirconia.

The starting point is zirconium dioxide (ZrO_2), also called zirconia. Zirconia exhibits three distinct structural phases as a function of temperature, as illustrated in Fig. 3.4. There is a monoclinic phase in the temperature range $0\,\mathrm{K} < T < 1{,}443\,\mathrm{K}$, a tetragonal phase in the temperature range $1{,}443\,\mathrm{K} < T < 2{,}633\,\mathrm{K}$, and a cubic phase at temperatures $T > 2{,}633\,\mathrm{K}$. We focus on the high temperature cubic phase, which has the fluorite structure in which the zirconium atoms form a face-centred cubic (fcc) sublattice and the oxygen atoms occupy all eight tetrahedral interstices in the fcc lattice. As such, the conventional cubic unit cell shown in Fig. 3.4 has eight O^{2-} ions and four Zr^{4+} ions, resulting in a charged balanced configuration.

Doping zirconia with yttrium atoms leads to the stabilisation of the cubic phase of zirconia at much lower temperatures compared to pure zirconia, and in particular the cubic phase can be stabilised at room temperature. The substitution of Zr^{4+} ions with Y^{3+} ions would break charge balance, which is compensated by the creation of O^{2-} vacancies. Overall, for every two Zr^{4+} ions replaced by two Y^{3+} ions, and oxygen O^{2-} vacancy is created. The resulting structure is depicted in Fig. 3.5, in which the partially green-grey balls represent the zirconium (green) and

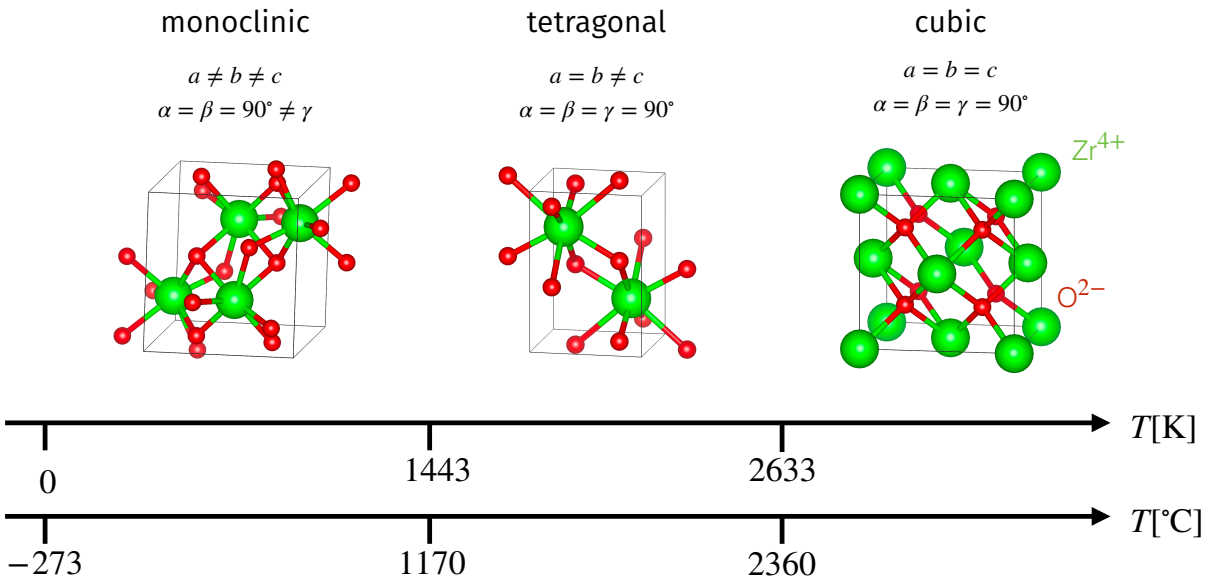

Figure 3.4: Structural phase diagram of zirconia as a function of temperature.

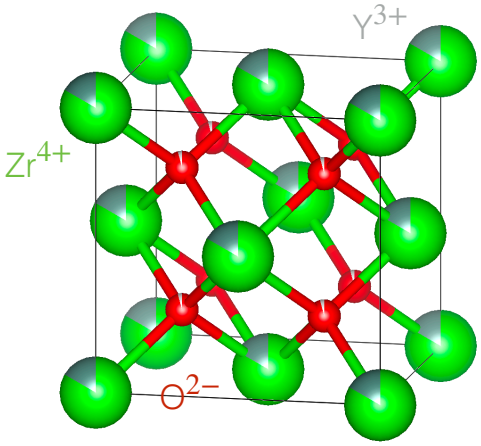

Figure 3.5: Structure of yttria-stabilised zirconia.

yttrium (grey) sites and the partially red-white balls represent the oxygen (red) and vacancy (white) sites. The volume of a ball occupied by a given colour represents the relative abundance of the corresponding species on that site.

The presence of oxygen vacancies in yttria-stabilised zirconia is key to the ionic conduction present in this compound. The O^{2-} ions move around the structure through the vacancy sites, and as a result yttria-stabilised zirconia is a prominent example of an ionic conductor.

3.2.2 Bismuth oxide

Another example of an ionic conducting material is bismuth oxide in its cubic δ-Bi_2O_3 phase. In this section, we introduce the structure of δ-Bi_2O_3.

Bismuth oxide exhibits a complex phase diagram as a function of temperature. The cubic δ-Bi_2O_3 phase occurs at temperatures above 1,002 K upon heating, but then survives to temperatures of 923 K or 912 K upon cooling, with the precise temperature depending on the cooling rate. In cubic δ-Bi_2O_3, the bismuth atoms form a fcc sublattice. Of the eight tetrahedral interstices in the conventional fcc unit cell, only six are occupied by oxygen, as required by charge balance between the Bi^{3+} and O^{2-} ions. As a result, δ-Bi_2O_3 natively has two oxygen vacancy

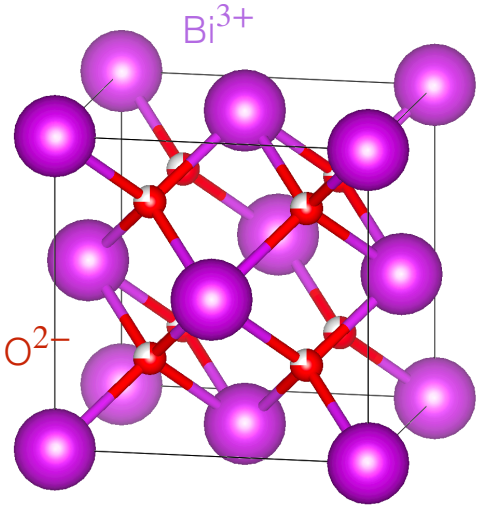

Figure 3.6: Structure of δ-Bi_2O_3.

sites in every conventional fcc unit cell. There is some dispute in the scientific literature about the precise structure of δ-Bi_2O_3, with one model suggesting that oxygens occupy ideal tetrahedral interstice sites of the fcc structure, while a competing model suggests that the oxygen sites are displaced from the ideal tetrahedral interstice sites of the fcc structure. Either way, the charge balance is the same and there are an average of six oxygens and two vacancies per conventional unit cell.

As in the case of yttria-stabilised zirconia, the presence of oxygen vacancies in δ-Bi_2O_3 is key to the ionic conduction present in this compound. Again, the O^{2-} ions move around the structure through the vacancy sites, and δ-Bi_2O_3 is another prominent example of an ionic conductor.

3.3 Applications of ionic conductors

Ionic conductors find applications in many different technologies. In this section, we will discuss two such applications: oxygen concentration cells and fuel cells.

3.3.1 Oxygen concentration cells

An oxygen concentration cell is a device used to measure the concentration of oxygen on an unknown sample. Its basic architecture is presented in Fig. 3.7, and we discuss it in some detail next.

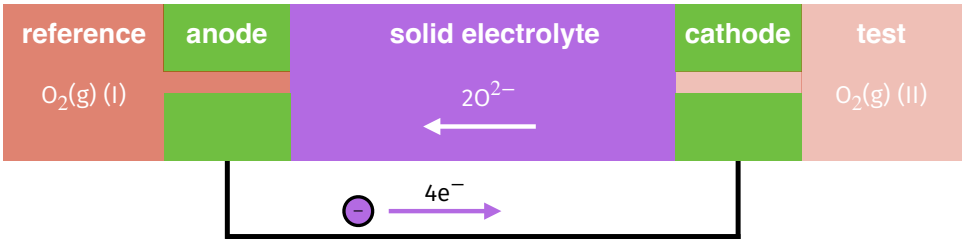

Figure 3.7: Schematic diagram of an oxygen concentration cell.

The core of an oxygen concentration cell is made of a solid electrolyte sandwiched between an anode and a cathode. The solid electrolyte is an ionic conductor such as yttria-stabilised zirconia

(YSZ), that allows the motion of ions but not the motion of electrons. The anode and cathode are metals that conduct electricity through the motion of electrons, with current entering the device through the anode and exiting through the cathode. A typically used metal is platinum Pt. The anode and cathode are connected to an external circuit through which electrons can flow (remember that electrons are negatively charged and flow in the opposite direction to the current).

The oxygen cell operates by interacting with a reference sample in contact with the anode and a test sample in contact with the cathode. The reference sample is a sample with a known oxygen partial pressure $O_2(g)(I)$, whereas the test sample has an unknown oxygen partial pressure $O_2(g)(II)$. The anode and cathode need to be porous to allow oxygen gas to flow through them and reach the solid electrolyte, which then leads to the schematic representation of an oxygen concentration cell as:

$$\mathrm{Pt(s)|O_2(g)(I)|YSZ|O_2(g)(II)|Pt(s)}.$$

Consider a case in which the oxygen partial pressure of the reference sample is smaller than the oxygen partial pressure of the test sample, $p\mathrm{O_2(g)(I)} < p\mathrm{O_2(g)(II)}$. In this case, $\mathrm{O^{2-}}$ ions flow from the cathode to the anode through the electrolyte, with the following half-cell reactions:

$$\text{cathode (reduction):} \quad \mathrm{O_2(g)(II) + 4\,e^- \longrightarrow 2\,O^{2-}} \tag{3.12}$$

$$\text{anode (oxidation):} \quad \mathrm{2\,O^{2-} \longrightarrow O_2(g)(I) + 4\,e^-} \tag{3.13}$$

Under these conditions, a potential difference develops across the cell, and measuring it provides a quantification of the relative oxygen partial pressures of the reference and test samples. Specifically, from electrochemistry we have that the electrochemical cell potential E is given by:

$$E = -\frac{RT}{4F} \ln\left(\frac{p\mathrm{O_2(I)}}{p\mathrm{O_2(II)}}\right), \tag{3.14}$$

where $R = 8.314\,\mathrm{JK^{-1}mol^{-1}}$ is the gas constant, T is temperature, and $F = 9.649 \times 10^4\,\mathrm{C\,mol^{-1}}$ is the Faraday constant.

If the opposite case in which the oxygen partial pressures are $p\mathrm{O_2(g)(I)} > p\mathrm{O_2(g)(II)}$, then charge flows in the opposite direction and the anode and cathode labels switch.

Oxygen concentration cells are used as sensors in a variety of applications. An every-day example is in lambda sensors used in vehicle exhaust systems. Lambda sensors measure the difference between the exhaust and atmosphere oxygen partial pressures with the aim of ensuring complete stoichiometric conversion of fuel to minimise emissions. The relevant chemical reaction is:

$$\mathrm{C_8H_{18} + \frac{25}{2}\,O_2 \longrightarrow 8\,CO_2 + 9\,H_2O},$$

and non-stoichiometric conversion (e.g. low oxygen concentration) leads to more severe emissions in the form of compounds like CO and NO_x. Using the stoichiometric reaction and using the relative molecular masses (remember air is about $4N_2 : O_2$), stoichiometric combustion is obtained when the air-to-fuel ration is 14.6. In this context, we define the lambda ratio as:

$$\lambda = \frac{\text{measured ratio}}{14.6}, \tag{3.15}$$

and the aim is to have $\lambda = 1$. The measured λ is then used to decide whether the reaction is stoichiometric, and if not, then the fuel flow is adjusted accordingly to either add oxygen when fuel-rich or add fuel-burn. A schematic diagram relating the cell potential and the oxygen partial pressure is shown in Fig. 3.8.

In an oxygen concentration cell, partial pressure differences drive a potential difference which in turn drives ionic motion. The basic principle is the equilibration of oxygen concentration. It is also possible to apply an external potential to directly drive ionic motion, which enables ions to move from regions of low concentration to regions of high concentration. This can be used, for example, to purify molten metals by removing oxygen impurities from them.

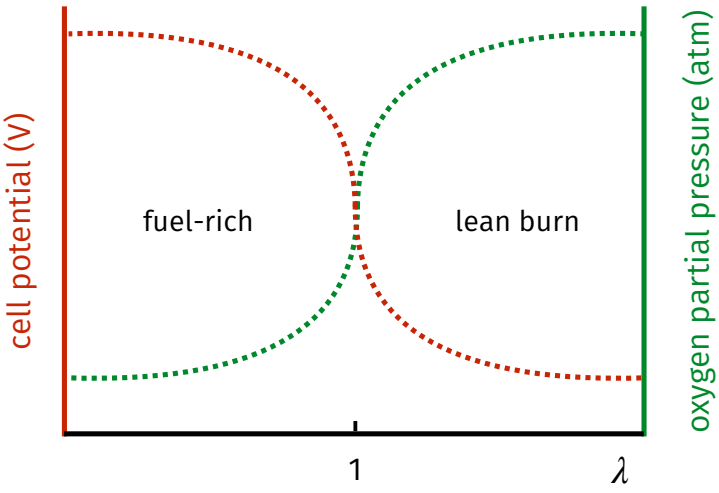

Figure 3.8: Schematic diagram of the cell potential and oxygen partial pressure and their relation to the λ parameter.

3.3.2 Fuel cells

In a typical gas-fired power station, the chemical energy of the fuel (typically CH_4) is converted into useful electrical energy through a series of steps that involve burning the fuel (chemical to thermal energy) whose steam then spins a turbine (thermal to mechanical energy) which then drives an electrical generator (mechanical to electrical energy). Energy is dissipated at every step of the process, making the overall operation of a gas-fired power station energy inefficient. A fuel cell, whose operation is based on the properties of ionic conductors, directly converts chemical energy into electrical energy, providing significant energy efficiency gains. Additionally, the use of hydrogen fuel eliminates nocive emissions. Put together, fuel cells are a promising technology for sustainable energy generation.

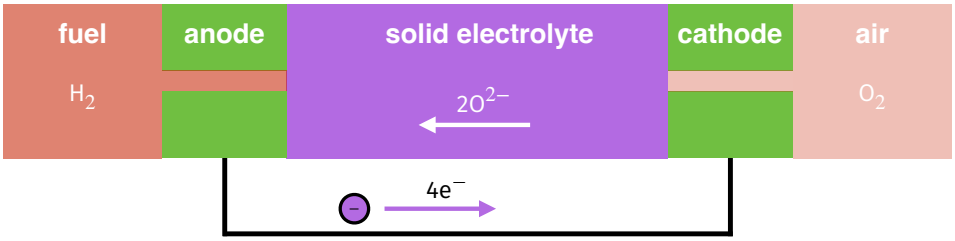

Figure 3.9: Schematic diagram of a hydrogen fuel cell.

The basic architecture of a fuel cell is depicted in Fig. 3.9. It is made of a solid electrolyte sandwiched between an anode and a cathode. The solid electrolyte is an ionic conductor such as yttria-stabilised zirconia (YSZ), that allows the motion of ions but not the motion of electrons. The anode and cathode are metals that conduct electricity through the motion of electrons, and must be porous to allow gas flow. Additionally, the cathode must be made of a material resistant to oxidation.

A hydrogen fuel cell uses hydrogen H_2 as the fuel, which reacts with oxygen from the atmosphere, and generates electrical energy from the electrons travelling through the external circuit. The solid electrolyte mediates the motion of oxygen from air to the anode. The half cell reactions are:

$$\text{cathode (reduction):} \quad O_2 + 4\,e^- \longrightarrow 2\,O^{2-} \tag{3.16}$$

$$\text{anode (oxidation):} \quad 2\,H_2 + 2\,O^{2-} \longrightarrow 2\,H_2O + 4\,e^- \tag{3.17}$$

The overall cell reaction is:

$$2\,H_2 + O_2 \longrightarrow 2\,H_2O. \tag{3.18}$$

Overall, a hydrogen fuel cell uses hydrogen and oxygen as inputs, and the only end product is water, generating no polluting emissions.

It also possible to use natural gas (methane) as the fuel, in which case the overall cell reaction is $CH_4 + 2\,O_2 \longrightarrow CO_2 + 2\,H_2O$. And it is also possible to use polymer-based electrolytes, whose ionic conduction is mediated by H^+ rather than O^{2-}.

Fuel cells have a number of advantages compared to competing technologies. Irrespective of the fuel used, the direct conversion of chemical to electrical energy makes a fuel cell about twice as efficient as an internal combustion engine. Additionally, if hydrogen is used as fuel, no polluting emissions are generated. Finally, the lack of mechanical parts reduces noise pollution. However, hydrogen fuel cells also present some challenges, highlighting the difficulty in generating and storing hydrogen, and the fact that hydrogen is highly flammable.

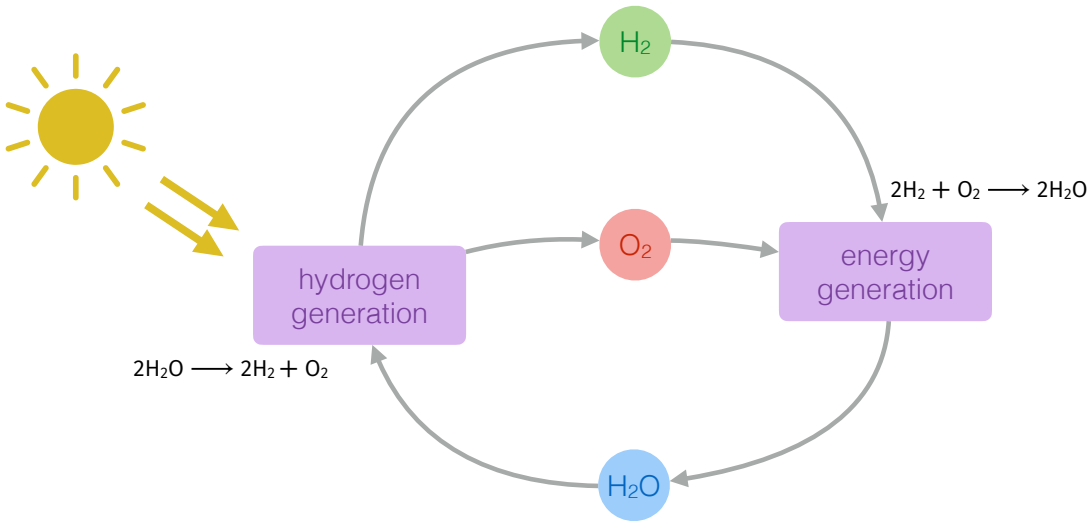

Figure 3.10: Schematic diagram of the hydrogen economy.

Hydrogen fuel cells could become part of what is called the *hydrogen economy*, schematically shown in Fig. 3.10. The vision is that solar energy can be used to split water and generate hydrogen. This hydrogen is then transported to the energy generation site, where it is used in a fuel cell, for example in a car or a factory. The operation of the fuel cell only generates water, that is released into the atmosphere and the cycle can start again. While this vision is appealing, there are many challenges to make it a reality. These include the fact that the generation of hydrogen from water (electrolysis) is an energy-intensive process and for it to be sustainable the energy source should itself be sustainable. Solar energy is a clear option, but the splitting of water using solar energy is an open scientific question. The other main challenge is the storage and transport of hydrogen, which requires compressed or liquified gas, again a very energy intensive process. Porous materials such as metal-organic frameworks are being actively investigated for hydrogen storage, but this is also an open scientific question.

Chapter 4

Liquid crystals

A crystalline solid is a material in which atoms are ordered in a regular pattern. This results in a periodic lattice with long-range order and properties that are anisotropic as they depend on the direction within the material. By contrast, a liquid is a system in which atoms are disordered, and as a result its properties are isotropic. Solids and liquids have very different properties, for example a liquid flows easily whereas a solid does not.

In this Chapter we introduce liquid crystals, materials whose properties are intermediate between those of crystalline solids and liquids. Liquid crystals are often made of elongated rod-like molecules such as polymers, and find applications in many areas including in light-based technologies such as liquid crystal displays.

4.1 Polymers

A *polymer* is a material made of large molecules composed of many repeating units, called *monomers*. Polymers are a vast class of compounds whose structural and chemical diversity endows them with a wide range of properties. Consequently, they find application from everyday life (clothing, packaging, construction, etc.) to advanced technologies (transistors, diodes, holography, etc.). Some polymers exhibit liquid crystal phases, and for this reason we introduce polymers in this Section.

4.1.1 Overview of polymers

A prominent example of a polymer is *polyethylene*, whose monomer is ethylene (ethene). Ethylene is the simplest alkene and it adopts a planar configuration. The structure of ethylene is shown in Fig. 4.1 using two alternative representations: a three-dimensional ball-and-stick representation (left) and a planar representation (right).

Figure 4.1: Structure of the ethylene molecule.

The polymerisation of ethylene leads to polyethylene, shown in Fig. 4.2. The structure is shown using three alternative representations: a planar representation (top), a compact planar representation (middle), and a three-dimensional ball-and-stick representation (bottom). The

subindex n in the compact planar representation indicates the number of times the monomer is repeated, and it is understood that the planar representation may extend at both ends to complete the full chain length if it does not fit within the page. The three-dimensional ball-and-stick representation clearly illustrates that polyethylene is not a planar polymer.

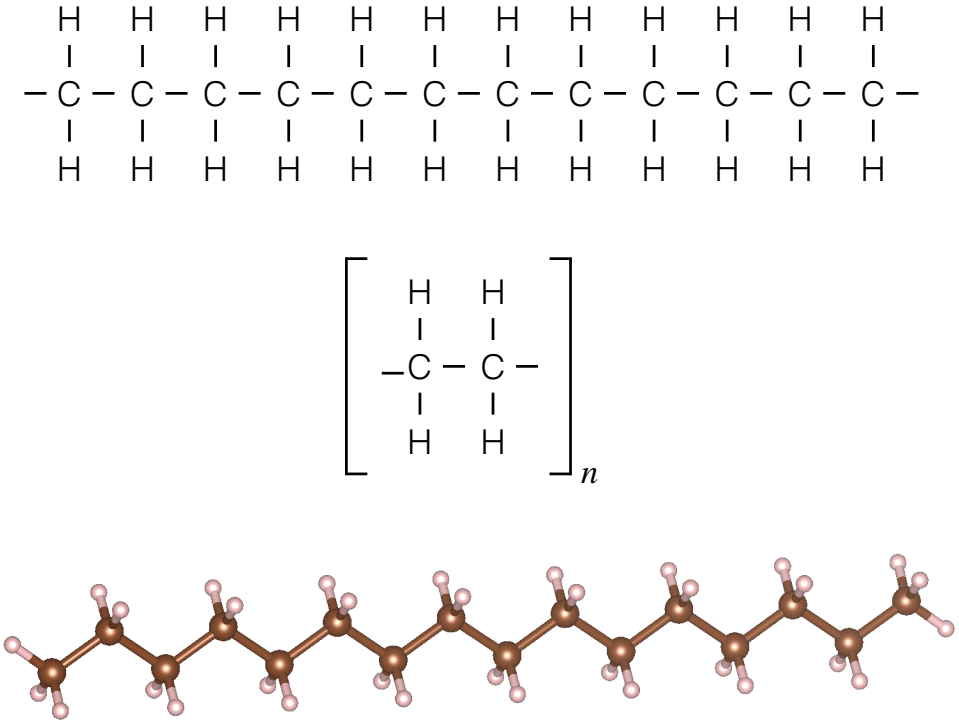

Figure 4.2: Structure of the polymer polyethylene.

Many different forms of polyethylene can be synthesised by controlling polymerisation conditions such as pressure and temperature. Several important forms are depicted in Fig. 4.3. The low density form of polyethylene (left diagram in Fig. 4.3) was the first one to be made historically, and can be made using high pressure synthesis techniques. It exhibits a significant amount of branching, which reduces intermolecular interactions and suppresses close-packing. The high density form of polyethylene (centre diagram in Fig. 4.3) can be made using transition metal catalysts that reduce side reactions. It has a single-chain configuration that enables close-packing, which leads to a high strength-to-density ratio. The cross linked form of polyethylene (right diagram in Fig. 4.3) can be made by high energy radiation or peroxide-mediated radical coupling. Its structure gives it reduced hardness and rigidity, and it exhibits high temperature stability and wear resistance.

These forms and additional forms find many applications, and indeed polyethylene is the most commonly produced plastic. Its low density form is used in trays, plastic bags, car parts, etc. Its medium density form is used in water plumbing. Its high density form is used in plastic bottles, corrosion resistant piping, etc. Its ultra-high molecular weight form is used in fibres and medical implants. Its cross-linked form is used in domestic water plumbing, insulation for high voltage electrical cables, etc. Its linear low-density form is used in plastic bags, toys, lids, etc.

Beyond the structural variations described above, polymers such as polyethylene also support chemical variations. For example, polypropylene is another polymer whose monomer is similar to that of polyethylene but one H side group is replaced by a CH_3 side group. The properties of polypropylene are similar to those of polyethylene, but it is slightly harder and more heat resistant. Polypropylene is the second most widely produced polymer plastic, and finds applications in furniture, lab equipment, clothing, etc. Another example is polyvinyl chloride (PVC), in which one H side group in polyethylene is replaced by a Cl side group. PVC is the third most

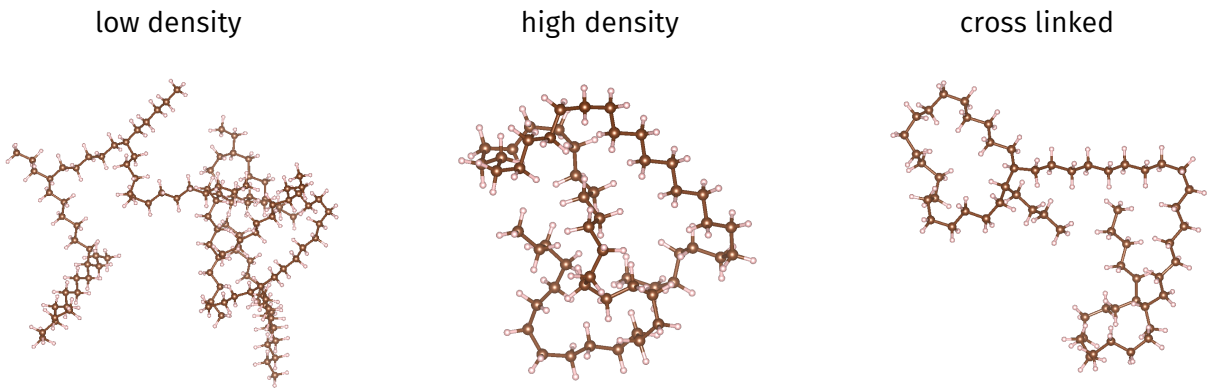

Figure 4.3: Alternative structural forms of polyethylene.

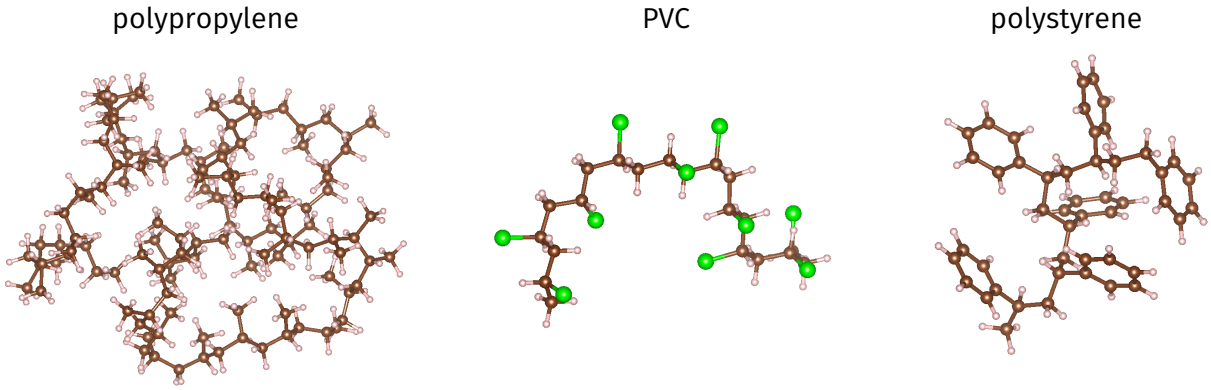

Figure 4.4: Structures of polypropylene (left), polyvinyl chloride (centre), and polystyrene (right).

widely produced polymer plastic, whose rigid form is used in pipes, door and window frames, etc, and its flexible form is used in electrical cable insulation, flooring, etc. As a final example, polystyrene is obtained by replacing one H side group in polyethylene by a C_6H_5 side group, giving another widely used polymers with applications in packaging, bottles, trays, disposable cutlery, etc. The structures of these three polymers are shown in Fig. 4.4.

4.1.2 Polymer structure

A simple model of the structure of polymers can be built by studying the mathematical construction known as a *random walk*. Consider a chain made of n segments each of length l, as shown in Fig. 4.5. Such a chain can be generated with a random walk, where each segment $\mathbf{r}_i$ has fixed length $|\mathbf{r}_i| = l$, but can point in any direction with equal probability. Indeed, a key property of this construction is that the direction of each segment of the chain is uncorrelated from the direction of other segments.

We define the countour length L as the total length of the chain:

$$L = nl. \tag{4.1}$$

We also define the vector $\mathbf{R}_i$ as the vector between the start of the chain and the end of segment $\mathbf{r}_i$, so that:

$$\mathbf{R}_i = \sum_{j=1}^{i} \mathbf{r}_j. \tag{4.2}$$

As examples, the vectors $\mathbf{R}_n$ and $\mathbf{R}_{n-1}$ are shown in Fig. 4.5. The vector $\mathbf{R}_n$ is called the *end-to-end vector* of the chain.

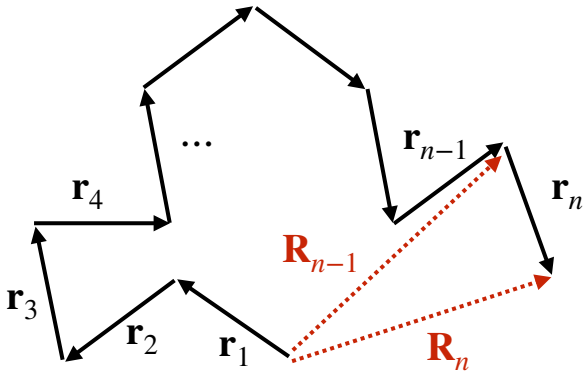

Figure 4.5: Example of a random walk.

To characterise the size of a chain like that in Fig. 4.5, we consider an ensemble of random walks of contour length L. The average $\langle \mathbf{R}_n \rangle = 0$ does not provide a good measure for the chain size, as any vector $\mathbf{R}_n$ in the ensemble is as likely as the opposite vector $-\mathbf{R}_n$, leading to the vanishing average. Instead, we consider the mean square end-to-end distance, which can be shown to be:

$$\langle \mathbf{R}_n^2 \rangle = nl^2. \tag{4.3}$$

From this, we define the *end-to-end distance* as:

$$\sqrt{\langle \mathbf{R}_n^2 \rangle} = l\sqrt{n}. \tag{4.4}$$

The end-to-end distance provides a simple quantification of the typical size of a chain generated using a random walk.

How can we use these ideas to understand the structure of polymers? Comparing the random walk in Fig. 4.5 with the polymer structures in Sec. 4.1.1, we see that they have similar shapes. This suggests that we can build a simple model for a polymer as a random walk. A key question is what polymer length should be associated with the length l of the steps in the random walk. Remember that the segments l in a random walk are uncorrelated, which implies that l cannot represent the carbon-carbon bond length, as the assumption of uncorrelated segments does not apply for carbon-carbon bonds. It turns out that there is no universal unit in polymers that we can assign to the random walk segment length l. Instead, each polymer will have different features, and we define a new quantity, the *Kuhn length*, as the length of a segment of polymer that is uncorrelated to other segments. As such, the Kuhn length of a polymer can be taken to be the segment length l in the random walk model. Table 4.1 shows the Kuhn lengths of some typical polymers.

Table 4.1: Examples of Kuhn lengths for selected polymers.

Polymer	**Number of monomers per Kuhn segment**
Polyethylene	5.7
Polypropylene	5.9
Polyvinyl chloride (PVC)	7.6
Polystyrene	10.8
DNA	600

4.2 Birefringence

The interaction of light with matter is a broad and diverse topic that encompasses areas as diverse as spectroscopy, lasers, and quantum information processing. In this Section, we introduce the concept of birefringence, which refers to a property of some materials, including liquid crystals, in which light propagation is direction-dependent.

3Blue1Brown has a series of three videos covering some of the discussion in this Section, which are a nice visual approach to the topic. The first video covers the experimental observations of light travelling between crossed polarisers, and subsequent videos go into the basics of polarised light and of the index of refraction.

4.2.1 Light-matter interactions

An *electromagnetic wave* is a wave that consists of oscillating electric and magnetic fields that propagate through space, as schematically shown in Fig. 4.6. Depending on their frequency, electromagnetic waves are classified as radio waves, microwaves, infrared, visible light, ultraviolet, X-rays, and gamma rays, and together form the electromagnetic spectrum. In this Section, we will often refer to electromagnetic waves as "light" because we are often interested in electromagnetic waves of frequencies corresponding to visible light.

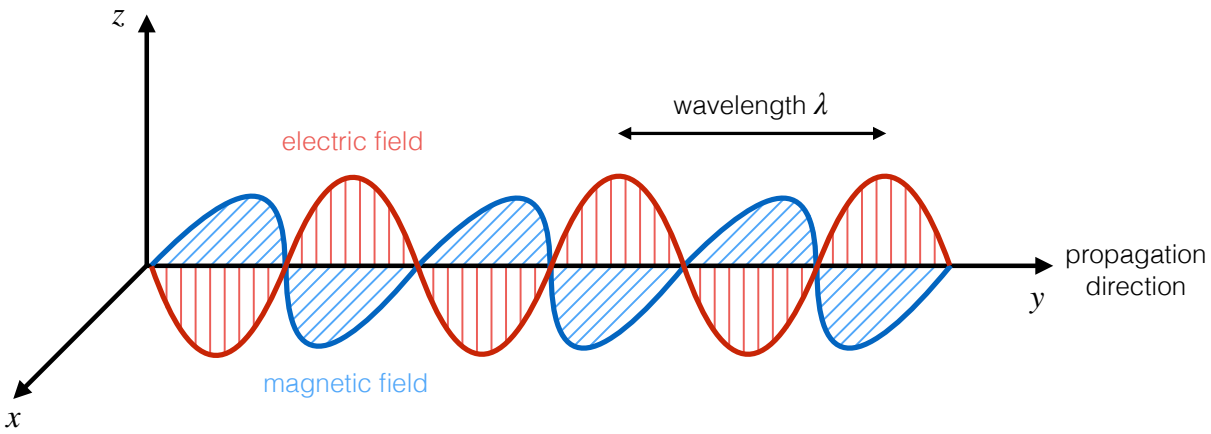

Figure 4.6: Schematic diagram of a monochromatic electromagnetic wave.

Monochromatic electromagnetic waves are electromagnetic waves of a single frequency. They can be characterised by their *wavelength* λ, which gives the length between successive maxima (or minima or any other pair of equivalent points) along the wave (see Fig. 4.6). The wavelength λ is related to the frequency f through the velocity v according to:

$$v = f\lambda. \tag{4.5}$$

The speed of light in vacuum is a constant $c = 299{,}792{,}458\,\mathrm{ms}^{-1}$ and represents a universal upper speed limit. When light travels through matter, its speed is smaller than the speed of light in vaccum $v < c$. Another important quantity for an electromagnetic wave is the *propagation direction*, which is perpendicular to the oscilation directions of both the electric and magnetic fields. In turn, the electric and magnetic fields are also perpendicular to each other (see Fig. 4.6).

The strongest interaction of light with matter is due to the electric field component, and we will neglect the magnetic field component of electromagnetic waves moving forward. We therefore consider the situation depicted in Fig. 4.7, in which we only have the electric field component of the electromagnetic wave. Figure 4.7 shows the same electric field component of an electromagnetic wave from two different directions. We define the *wave polarisation direction* as the direction of the oscillating electric field, such that in the diagrams in Fig. 4.7 it is along

the z axis. Do not confuse the polarisation of a wave with the electric polarisation discussed in Chapter 1.

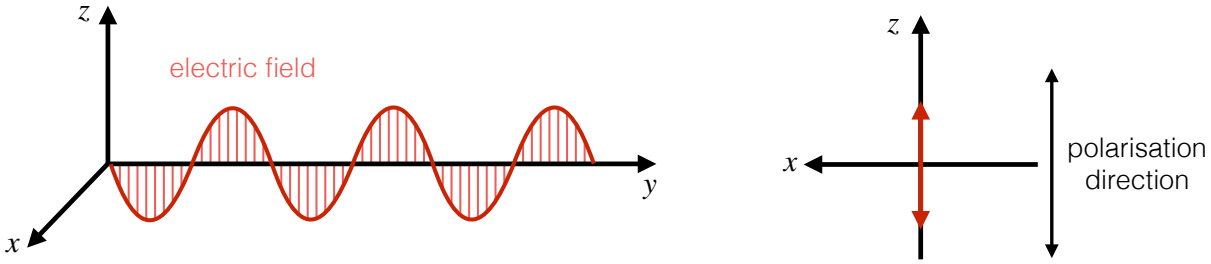

Figure 4.7: Schematic diagram of a monochromatic electromagnetic wave highlighting the electric field component.

Light associated with an electromagnetic wave with a single wave polarisation direction is called *polarised light*, and a schematic example is depicted in the left diagram of Fig. 4.8. Instead, if an electromagnetic wave has electric field oscillations in many different directions, then we refer to it as *unpolarised light*. A schematic example of unpolarised light is shown in the right diagram of Fig. 4.8. Most light sources, such as the Sun, flames, or lamps, generate unpolarised light. To illustrate this concept, we consider sunlight as an example. In the Sun, nuclear reactions heat up the atomic nuclei and electrons making up the solar plasma. From electromagnetism, accelerating charged particles emit electromagnetic waves, and in the sun each emission occurs in a random direction, resulting in unpolarised light.

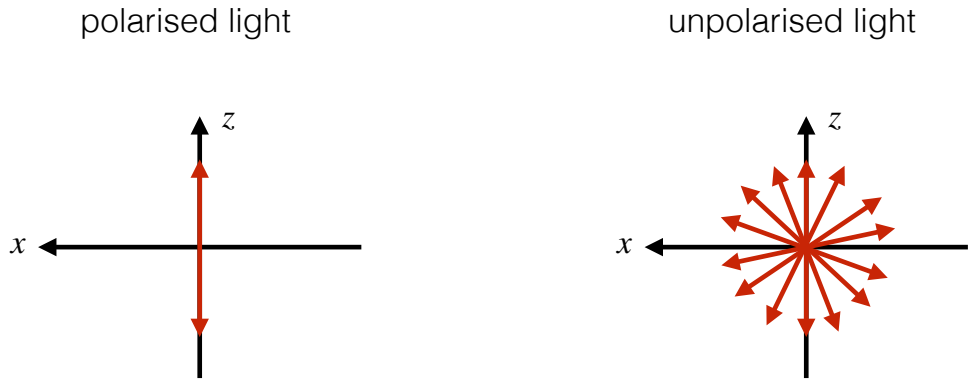

Figure 4.8: Schematic diagram comparing the polarisation direction of polarised light (left) and unpolarised light (right).

As briefly introduced earlier, the speed of light in vacuum c is a universal upper speed limit, and has a value of $299{,}792{,}458\,\mathrm{ms}^{-1}$. When light travels through matter, its speed v is smaller than the speed of light in vacuum. We introduce the dimensionless *refractive index* n as the ratio of the two:

$$n = \frac{c}{v}. \tag{4.6}$$

As the speed of light in vacuum is an upper limit, we have that $n \geq 1$, and the larger the refractive index the slower the speed of light in the material. Microscopically, when light travels through matter its oscillating electric field drives the oscillation of the electrons in the material. Oscillating charges emit their own electromagnetic waves, and light in the material becomes the superposition of the original wave and the waves emitted by the oscillating electrons. The electromagnetic waves emitted by the electrons are typically of the same frequency as the driving wave, but with a shorter wavelength, leading to an overall reduction of the phase velocity of the wave such that $v < c$. As an additional feature, the response of the electrons in a material to

an oscillating electric field is frequency dependent, so the the speed of light in a material is also frequency dependent.

4.2.2 Light-polymer interactions

The elongated quasi-one-dimensional nature of polymers leads to different light-matter interactions along the different polymer axes. We define:

- Slow axis: light couples strongly in this direction so light is significantly slowed.
- Fast axis: light couples weakly in this direction, so light does not slow much.

Slow and fast axes are perpendicular to each other, and are collectively referred to as the *permitted vibration directions*.

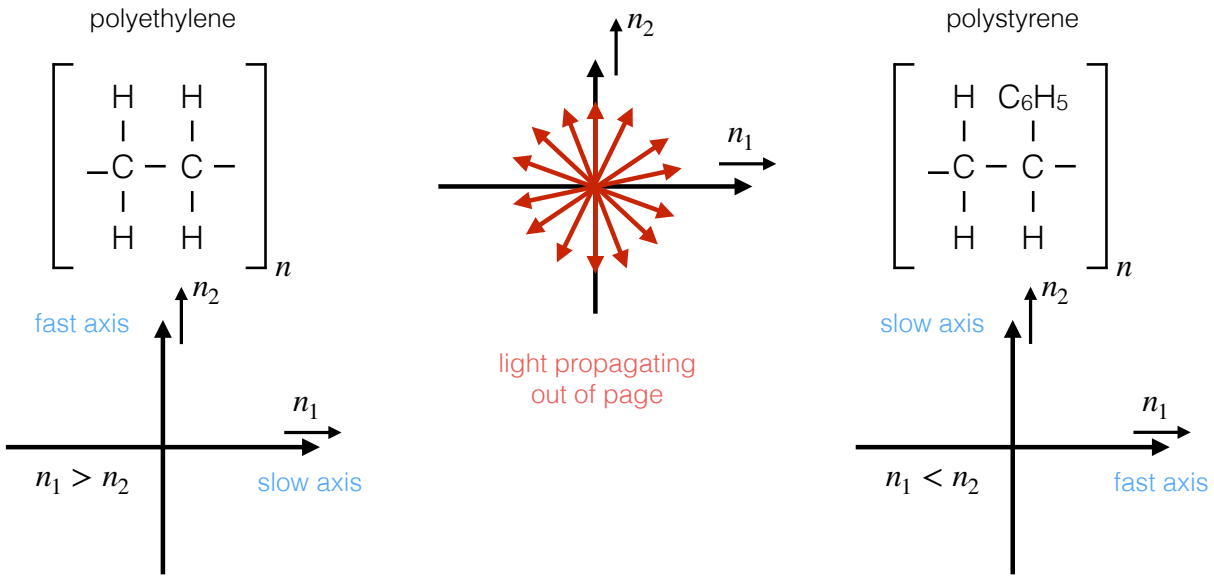

Figure 4.9: Schematic diagram comparing the slow and fast axes of polyethylene and polystyrene.

The nature of the slow and fast axes is material-dependent. For example, Fig. 4.9 schematically shows the slow and fast axes of two different polymers, polyethylene and polystyrene. We consider light with a propagation direction pointing out the page, and define the refractive index along the horizontal axis as n_1 and the refractive index along the vertical axis as n_2. We orient both polymers such that the long side of the chain is horizontal, and the short side is vertical. For polyethylene, the refractive index is larger along the chain $n_1 > n_2$, which means that light moves slower along the chain than perpendicular to it. For polystyrene we have the opposite situation: the refractive index is smaller along to the chain $n_1 < n_2$, which means that light moves faster along the chain than perpendicular to it.

4.2.3 Birefringence

Birefringence is the property of a material with a refractive index that depends on the polarisation and propagation directions of light. From our discussion in Sec. 4.2.2 about the slow and fast axes of polymers, we conclude that polymers exhibit birefringence. Quantitatively, the birefringence Δn is defined as:

$$\Delta n = n_1 - n_2, \tag{4.7}$$

where n_1 and n_2 are refractive indices along different directions in the material.

We have introduced the interaction of light with polymers in Sec. 4.2.2 by considering a single polymer chain. Polymer materials have many different polymer chains, and the birefringence of

the material depends on the ordering of these chains. For example, a sample in which the different polymer chains are randomly oriented will exhibit no birefringence because the relative fast and slow axes of each individual chain will be randomly oriented with respect to the corresponding axes of the other chains. Conversely, a material with polymer chains all oriented in the same direction will in general exhibit birefringence.

We have discussed in Sec. 4.2.1 how light from most common sources is unpolarised. We can transform unpolarised light into polarised light by using materials called *polarisers*. A polariser is a material that only allows light of a specific polarisation to pass through. As such, polarisers are an extreme example of birefringent materials. Figure 4.10 schematically shows the polarisation of light with a polariser. We conventionally represent a polariser (in blue in Fig. 4.10 with lines indicating thee direction of along which light is allowed to pass through, such that the resulting light polarisation is parallel to these lines.

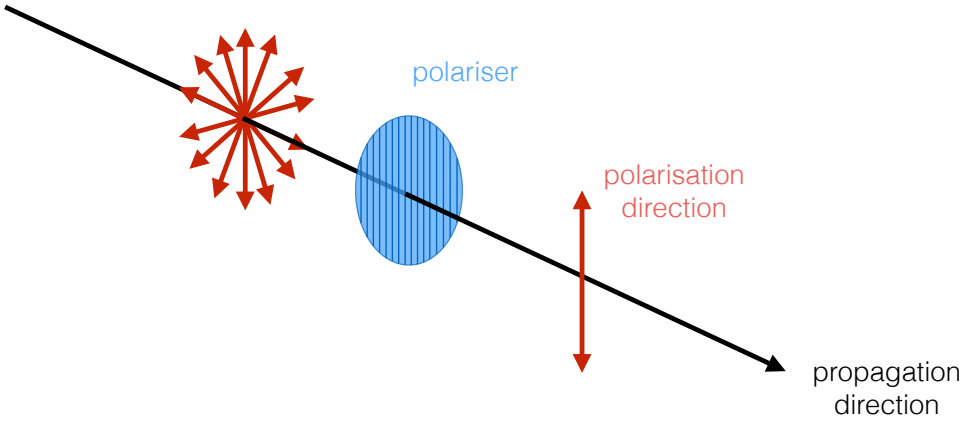

Figure 4.10: Schematic diagram of a polariser acting on initially unpolarised light.

We next investigate the interaction of polarised light with a birefringent material. Consider the setup illustrated in Fig. 4.11. The birefringent material (in green) has a rectangular prismatic shape, and the propagation direction of light is parallel to one of the prism sides of thickness l. We also include the polarisation direction of the incident light and the permitted vibration directions of the birefringent material, which in general are not aligned with the light polarisation.

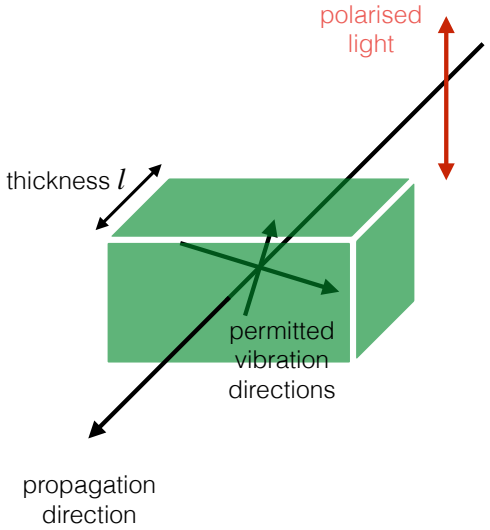

Figure 4.11: Schematic diagram of a polariser acting on initially unpolarised light.

In a general situation, light travelling at speed v will traverse a material of thickness l in a time $T = \frac{l}{v}$. Using the refractive index $n = \frac{c}{v}$, we can re-write the time as $T = \frac{ln}{c}$. For a

birefringent material, the two orthogonal permitted vibration directions have different refractive indices n_1 and n_2, and this leads to two different times for light travelling across the material, $T_1 = \frac{ln_1}{c}$ associated with n_1 and $T_2 = \frac{ln_2}{c}$ associated with n_2. The time difference is then:

$$\Delta T = T_1 - T_2 = \frac{l}{c}(n_1 - n_2) = \frac{l\Delta n}{c}. \tag{4.8}$$

The component of light travelling along the fast axis will exit the material a time ΔT earlier. During this time, it travels at speed c outside the material over a distance:

$$c\Delta T = c\left(\frac{l\Delta n}{c}\right) = l\Delta n. \tag{4.9}$$

We call this distance the *optical path difference* OPD:

$$\text{OPD} = l\Delta n. \tag{4.10}$$

It is often convenient to re-write the optical path difference in terms of a phase difference. Remember that the phase ϕ of a wave at position x with respect to position x_0 is given by $\phi = 2\pi\left(\frac{x-x_0}{\lambda}\right)$, where λ is the wavelength of light. This implies that the optical path difference between light along the slow and fast axes leads to a phase difference δ given by:

$$\delta = 2\pi\left(\frac{\text{OPD}}{\lambda}\right) = 2\pi\frac{l\Delta n}{\lambda}. \tag{4.11}$$

4.2.4 An example: birefringent sample between crossed polarisers

We can use Eqs. (4.10) and (4.11) to investigate the behaviour of birefringent materials placed between crossed polarisers. We consider the general situation depicted in Fig. 4.12 in which we have a birefringent material (green) placed between two crossed polarisers (blue) such that the polarisation of light allowed through the first polarisers is perpendicular to that allowed through the second polariser.

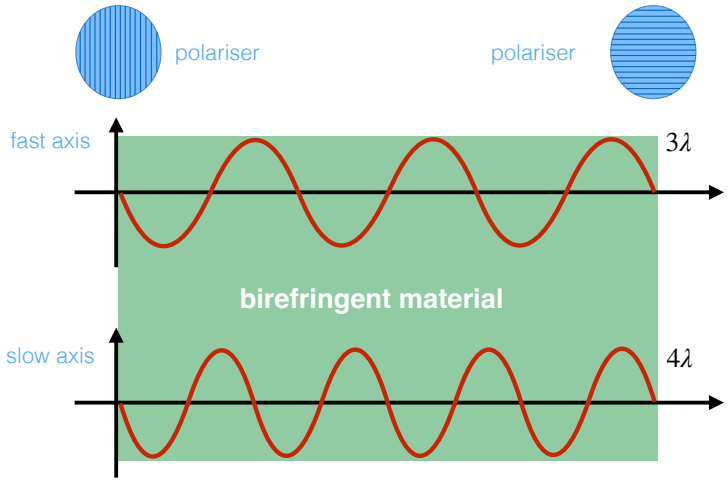

Figure 4.12: Schematic diagram of a cross polariser configuration with an optical path difference that is a multiple of the wavelength of light.

As a first example, consider a situation in which the optical path difference is a multiple of the wavelength OPD $= k\lambda$ for positive integer k, or equivalently a phase difference $\delta = 2\pi k$. This situation is depicted in Fig. 4.12. First note that, inside the birefringent material, the wavelength of light along the fast axis is larger than the wavelength of light along the slow axis.

To understand this, remember that the speed of light v is related to the light frequency f and wavelength λ by $v = \lambda f$. The frequency of light does not change in the material, so that:

$$n = \frac{c}{v} = \frac{\lambda_0 f}{\lambda f} = \frac{\lambda_0}{\lambda}, \tag{4.12}$$

where λ_0 is the vacuum wavelength. From this derivation, we obtain the following relationship:

$$n_{\text{slow}} > n_{\text{fast}} \implies \lambda_{\text{slow}} < \lambda_{\text{fast}}. \tag{4.13}$$

This implies that the wavelength of light is shorter along the slow axis compared to the fast axis, as schematically depicted in Fig. 4.12.

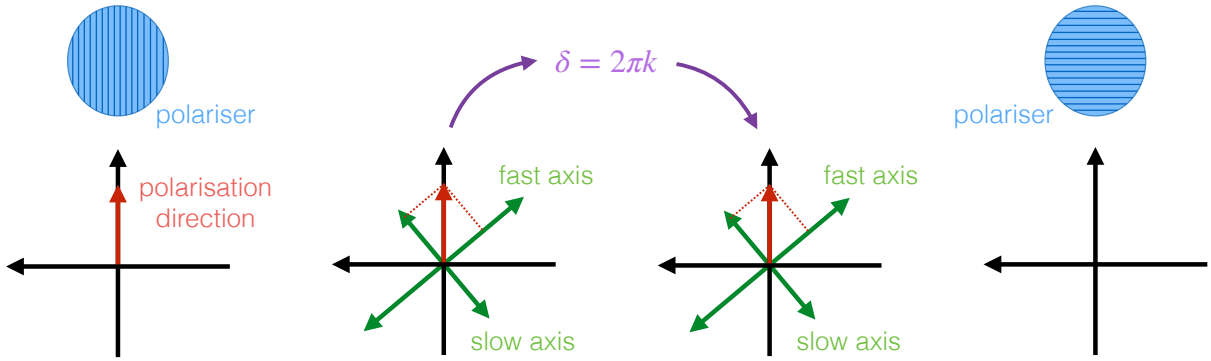

Figure 4.13: Schematic diagram of the polarisation direction of light as it transists through the cross polariser setup in Fig. 4.12.

The transit of ligth through this setup is depicted in Fig. 4.13. Light enters the material through the first polariser, so its polarisation direction is initially vertical (first diagram in Fig. 4.13). Inside the birefringent material, the light polarisation will in general not be aligned with the permitted vibration directions, so we can separate the oscillating electric field into its components along the fast and slow axes (second diagram in Fig. 4.13). At the end of the birefringent material, the two light components are again in phase with each other, as $\delta = 2\pi k$ (third diagram in Fig. 4.13). This means that the light polarisation is now perpendicular to the seconod polariser, so that overall no light will be allowed through the second polariser (fourth diagram in Fig. 4.13).

In Problem 15 we consider a second example in which the optical path difference is OPD $= k\lambda + \frac{\lambda}{2}$ for positive integer k, or equivalently a phase difference of $\delta = 2\pi k + \pi$. In this situation, light enters the birefringent material with polarisation aligned with the first polariser, but the phase difference that develops across the birefringent material leads to light exiting the birefringent material with a polarisation perpendicular to that of the original polariser. This new light polarisation is aligned with the second polariser, so light is allowed through. Overall, this second setup leads to light allowed through the cross-polarisers and the outgoing light has a polarisation perpendicular to the polarisation of the incoming light.

To generalise the two examples discussed above, we consider initially unpolarised white light. White light is light made of all possible wavelengths in the visible part of the electromagnetic spectrum. First note that the phase difference arising from the optical path difference across a birefringent material depends on the light wavelength according to $\delta = 2\pi \frac{l\Delta n}{\lambda}$. When a birefringent material is placed between cross polarisers, most wavelengths of white light will pass through as the phase difference δ will introduce a component of the initially polarised light in a perpendicular direction, which will be allowed through the second polariser. However, there will be one wavelength of light, corresponding to $\delta = 2\pi$, that will not pass through the second polariser. As a result, the observed spectrum will be equal to the original spectrum missing that one wavelength.

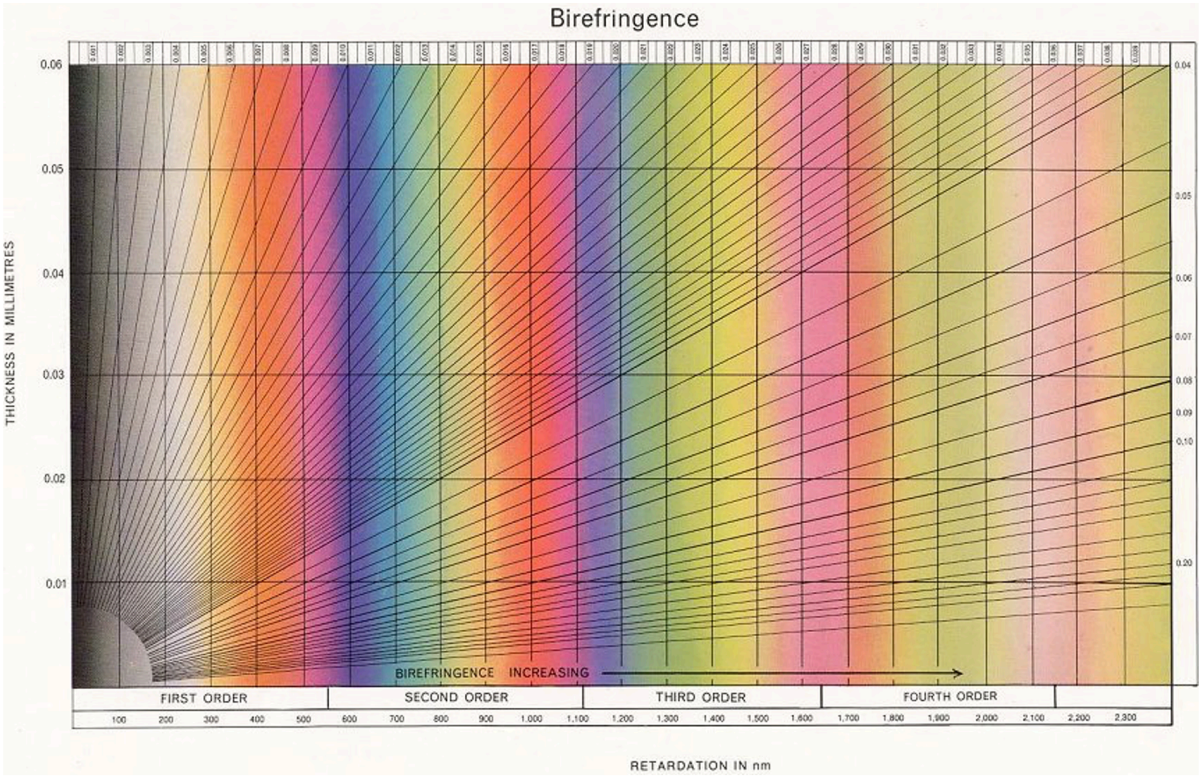

Figure 4.14: Michel-Levy chart. Source unknown.

The colour that is left when a frequency of light is removed is called the *complementary colour*. For example, the complementary colour of blue is yellow, that of green is magenta, and that of red is cyan. This leads to the construction known as the *Michel-Levy chart*, shown in Fig. 4.14. The horizontal axis of the Michel-Levy chart depicts the "retardation" (in nanometres), which is a synonym for the optical path difference OPD. The vertical axis depicts the thickness l of the sample (in milimetres). The sloped straight lines spreading from the origin depict the birefringence Δn, and its values are shown along the top and right axes of the diagram. The Michel-Levy diagram is used to extract the colour of initially white light that will be allowed through a sample of birefringence Δn, thickness l, and associated optical path difference (retardation), placed between crossed polarisers. For example, a material of thickness 0.03 mm and birefringence 0.05 will give a yellow-pink colour.

To understand the overall colour sequence of the Michel-Levy chart, we can use the insights above about white light travelling through a birefringent material placed between crossed polarisers. Starting with small optical path differences (left part of the Michel-Levy chart), there is very little rotation of the light and very little light is transmitted through the second polariser, resulting in a black-grey colour. Increasing the optical path difference, the first colour is yellow. Remember that yellow is the complementary colour of blue, so this implies that the wavelength of light that has been removed is that corresponding to blue. This is to be expected as blue has the shortest wavelength in the visible spectrum, and therefore the phase difference, which remember is $\delta = 2\pi \frac{l\Delta n}{\lambda}$ is largest for a given thickness and birefringence. Further increasing the optical path difference leads to a sequence of colours that correspond to the complementary colours of the visible part of the spectrum as the wavelength of the removed colour increases. Eventually we encounter yellow again, which corresponds to an optical path difference that is twice the wavelength of blue light, and the pattern repeats. The colours become less well-defined at every sequence of the chart because for longer optical path differences it becomes increasingly likely that several distinct wavelengths in the visible part of the spectrum will have a multiple that coincides with the path difference, so multiple wavelengths are removed at the same time.

Placing a birefringent sample between crossed polarisers and using the Michel-Levy chart can also be used to characterise the properties of an unknown birefringent material. If the initial polariser is aligned with the fast or slow axes, then no path difference will develop, and no light will be transmitted after the second crossed polariser. Such a position is called an *extinction position* and the sample appears black. Rotating a birefringent sample over a half-revolution will reveal two orientations along which it will appear black, and these correspond to the two extinction positions. Performing this experiment allows us to determine the two permitted vibration directions of the sample.

To determine which direction corresponds to the fast and slow axes, we use a second reference material of known birefringence, often called a compensator. We align the the permitted vibration directions of the unknown birefringent material with the compensator, and compare an the initial alignment with a second alignment which corresponds to a rotation by 90°. In one setup the two fast axes and the two slow axes will be fully aligned, and in the other setup the fast axes of each sample will be aligned with the slow axes of the other. The resulting optical path difference will be larger in the first case compared to the second, so the fast-fast and slow-slow alignment will give a higher colour in the Michel-Levy chart compared to the fast-slow and slow-fast alignment. This procedure therefore reveals the fast and slow axes of the initially unknown birefringent sample.

4.3 Liquid crystals

In this Section we introduce liquid crystals and look at some of their applications. From a structural point of view, liquid crystals are made of rod-like molecules of which polymers are a prominent example. From an application point of view, liquid crystals exhibit birefringence, and as a result they find application in light-based technologies such as liquid crystal displays.

4.3.1 Nematic liquid crystals

A liquid crystal is a state of matter with properties intermediate between those of a crystalline solid and a conventional liquid. Specifically, liquid crystals are anisotropic liquids. Depending on their structure, liquid crystals can be classified into several different classes, including nematic, smectic, and chiral nematic. In this Section, we investigate the properties of nematic liquid crystals.

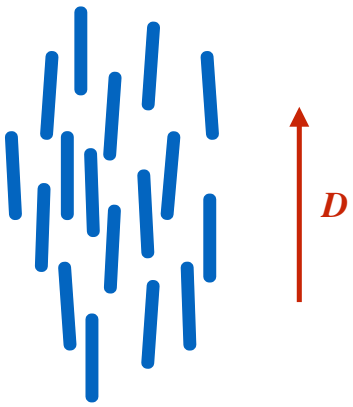

Figure 4.15: Schematic structure of a nematic liquid crystal.

A *nematic* liquid crystal is typically made of organic rod-like molecules. In this phase, the centres of mass of the molecules have no long range order and flow like a liquid. However, the molecules tend to align along some common axis, which can be described by a vector called the *director* **D** (see Fig. 4.15). The alignment along the director leads to anisotropic

properties analogous to those of a crystal. Do not confuse the symbol **D** for the director with the displacement field discussed in Chapter 1.

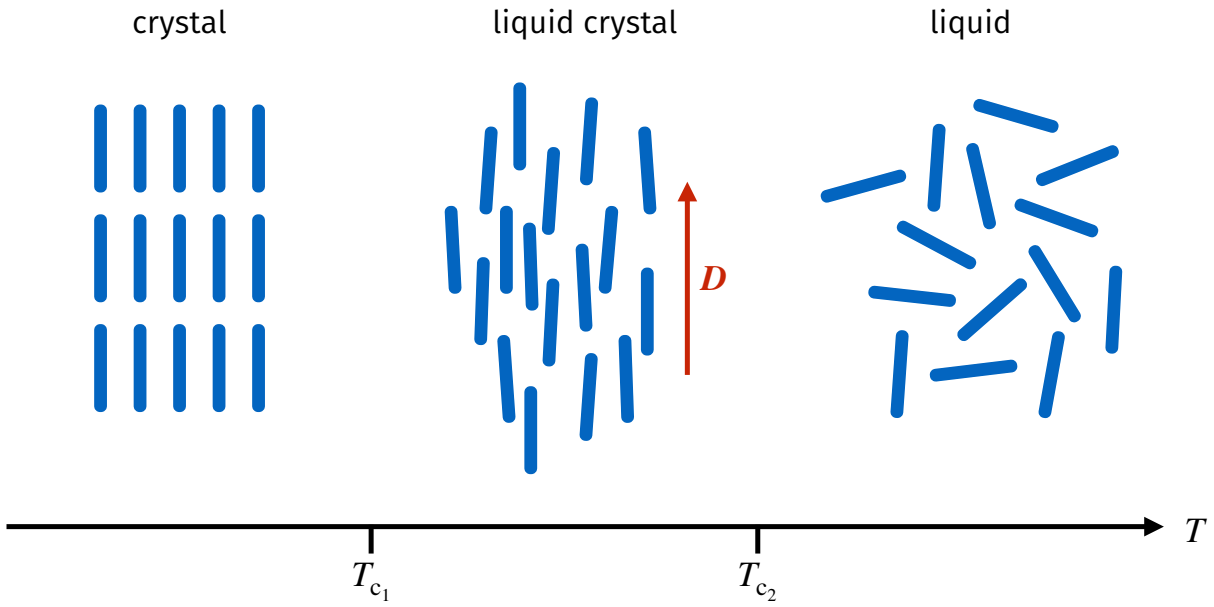

Figure 4.16: Phase diagram of a nematic liquid crystal.

Liquid crystals were first discovered as materials exhibiting *two* melting temperatures. Below a first critical temperature T_{c_1}, the material is ordered as a crystalline solid. Above a second critical temperature T_{c_2}, the material is disordered as a liquid. But at intermediate temperatures the material forms a liquid crystal characterised by a director **D** as described above. This phase diagram is depicted in Fig. 4.16, and is driven by a competition between rod-rod interactions that favour ordering and thermal energy that favours disordering.

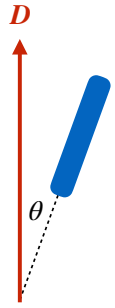

Figure 4.17: Definition of angle θ between a molecule and the director **D**.

To understand the properties of nematic liquid crystals we need to characterise their order. To simplify the problem, we are going to consider that the rod-like molecules making up the liquid crystal are cylindrical and have no internal structure, so that there is no "up" or "down" orientation. In principle, we could describe the order associated with a collection of molecules using a distribution function $f(\theta, \phi)$ giving the fraction of molecules pointing in any given direction (θ, ϕ), where these coordinates correspond to the standard angular spherical coordinates. However, it is more convenient to describe the order of the system with a single numerical parameter, and we introduce the *order parameter* Q, defined as:

$$Q = \frac{1}{2}\langle 3\cos^2\theta - 1\rangle, \tag{4.14}$$

where θ is the angle between a molecule and the director **D** as shown in Fig. 4.17, and the angle

brackets indicate an average over all molecules in the system. One can show that when all the molecules of the system are fully aligned, then $Q = 1$, and when they are randomly aligned $Q = 0$. Intermediate values of Q allow us to quantify the degree of disorder in the system. A more detailed discussion of these ideas is presented in Appendix C.

4.3.2 Classification of liquid crystals

Nematic liquid crystals discussed in Sec. 4.3.1 are only one possible class of liquid crystal. In this Section we briefly introduce two other classes of liquid crystal, smectic liquid crystals and chiral nematic liquid crystals.

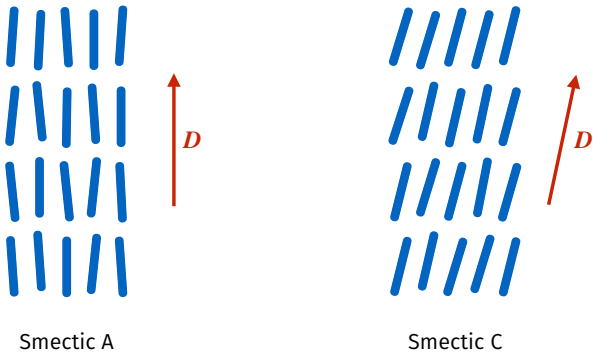

Figure 4.18: Schematic structure of smectic A (left) and smectic C (right) liquid crystals.

Smectic liquid crystals are liquid crystals in which the rod-like molecules organise in layers, as schematically depicted in Fig. 4.18. We can identify two types of smectic liquid crystal: smectic A liquid crystals have the director **D** parallel to the layer normal, and smetic C liquid crystals have the director **D** not parallel to the layer normal.

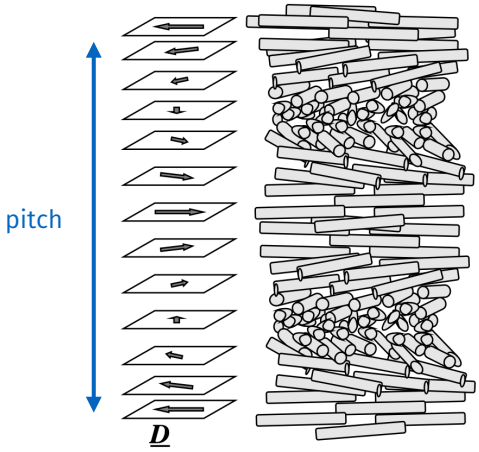

Figure 4.19: Schematic structure of a chiral nematic liquid crystal. Source unknown.

Chiral nematic liquid crystals, also referred to as cholesteric liquid crystals, are schematically depicted in Fig. 4.19. They have the director **D** parallel to a plane (a horizontal plane in Fig. 4.19), and the director rotates along this plane tracing out a helix. In this context, we define the *pitch* as the distance required for the director to perform a full 360° degree rotation. The pitch of a chiral nematic liquid crystal can vary anywhere between 100 nm to 100 μm depending on the molecules making up the liquid crystal, the degree of polymerisation, or the concentration in solution.

4.3.3 Birefringence in liquid crystals

The rod-like nature of the constituent molecules of liquid crystals naturally leads to birefringence. Taking a nematic liquid crystal as an example (refer back to Fig. 4.15), the permitted vibration directions are parallel and perpendicular to the director **D**. For example, the component of light travelling along the molecules (parallel to **D**) has a larger refractive index compared to a perpendicular direction.

It is important to note that the relative orientations of the light propagation direction and the nematic liquid crystal director **D** determine how birefringence manifests in a given sample. For example, for light with propagation direction along **D**, there is no birefringence as the cross-section of the liquid crystal molecules appears isotropic in that direction (remember that the polarisation of light is always perpendicular to the propagation direction, so in this example it is also perpendicular to the nematic liquid crystal director).

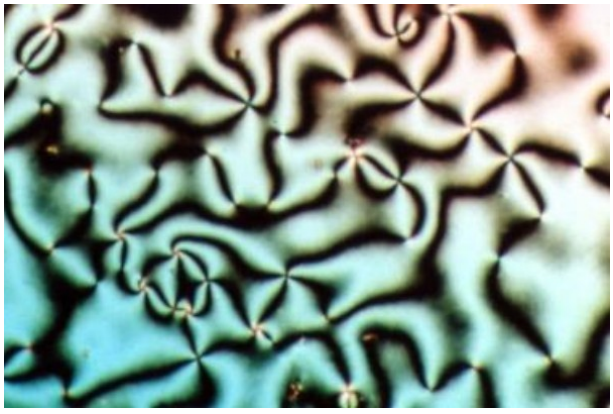

Figure 4.20: Schlieren texture characteristic of a nematic liquid crystal between crossed polarisers. Reproduced from Minutemen [CC BY-SA 3.0] via Wikimedia Commons.

We next consider the setup discussed in Sec. 4.2.4 with a birefringent material placed between crossed polarisers, with the special case of the birefringent material being a liquid crystal. Starting with a nematic liquid crystal, we note that real samples exhibit domains in which the director **D** points in different directions. The the resulting domain boundaries are called *disclinations*. A nematic liquid crystal placed between crossed polarisers shows the texture depicted in Fig. 4.20, and called *Schlieren texture*. Each bright region corresponds to a different domain, and the dark boundaries between them correspond to the special case in which the director is aligned with one of the cross polarisers or parallel to light propagation, as in both instances there is no light propagation through the setup.

We next consider a chiral nematic liquid crystal between crossed polarisers, and focus on the direction of propagation of light perpendicular to the helical axis, corresponding to going into or out of the page in the left diagram of Fig. 4.21. In this scenario, when **D** is parallel to the propagation direction of light there is no transmission, resulting in the dark fringes obesrved in Fig. 4.21. When **D** is not parallel to the propagation direction of light, then we observe birefringence leading to bright regions. Figure 4.21 shows a schematic diagram of the structure of a chiral nematic liquid crystal and the resulting bright and dark fringes, and also two realistic examples of birefringence from such samples (centre and right). The resulting textures resemble fingerprints.

4.3.4 Liquid crystal displays

One of the most prominent uses of liquid crystals is in liquid crystal displays (LCDs), used in wide range of applications including phones, televisions, computer monitors, calculators, and

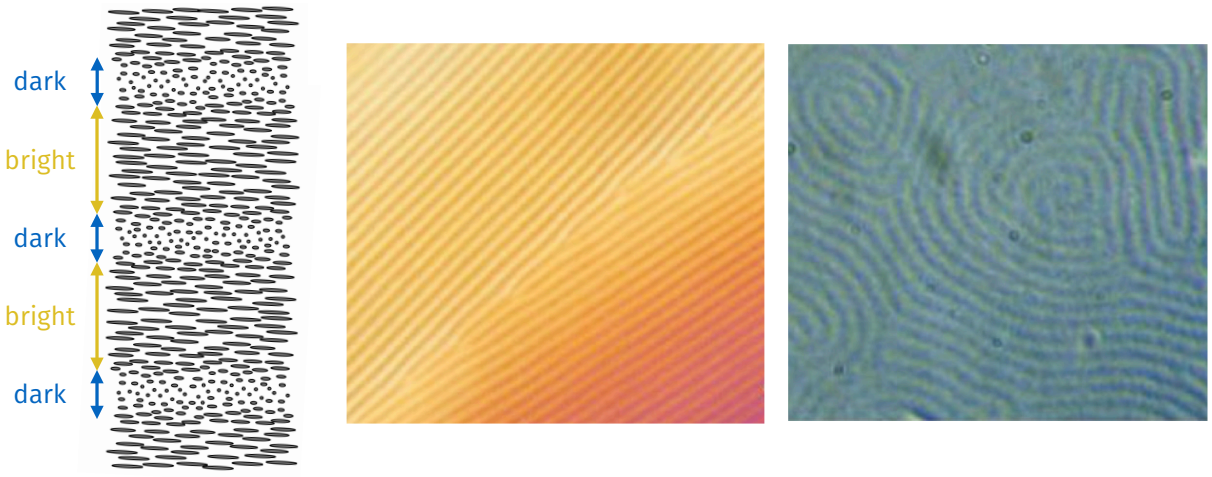

Figure 4.21: Fingerprint texture characteristic of a chiral nematic liquid crystal between crossed polarisers. Adapted from source unknown.

watches. In this Section we describe the basic principles behind the operation of liquid crystal displays.

The director **D** of a nematic liquid crystal can be forced to lie along a particular direction by placing it in contact with a surface that has grooves in that particular direction. If the nematic liquid crystal is sandwiched between two plates with their respective grooves aligned perpendicularly, then the director twists across the sandwich and we end up with a *twisted nematic structure*. We consider such a twisted nematic structure placed between crossed polarisers, such that each polariser is aligned with the director at its end, as schematically shown in Fig. 4.22.

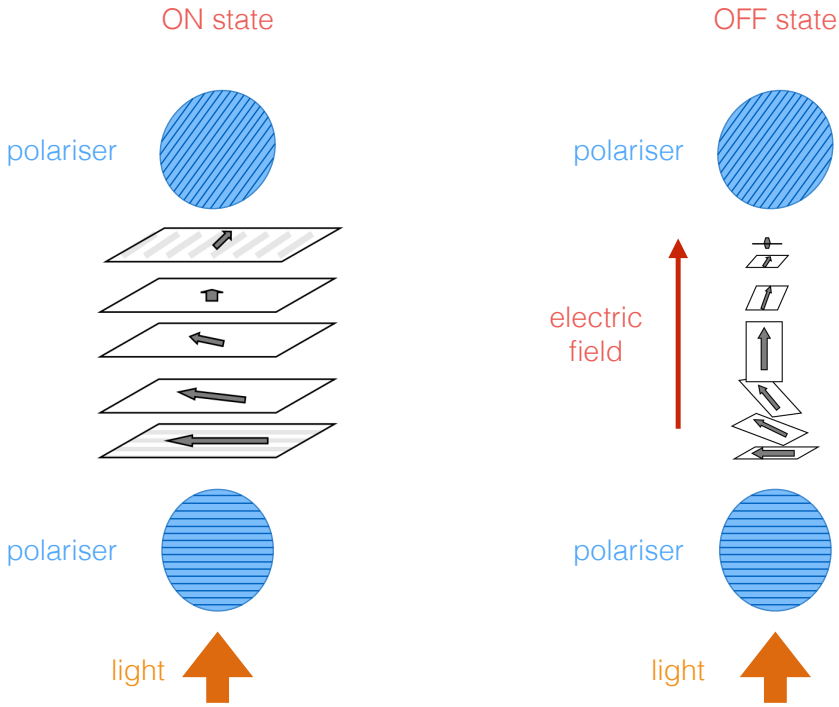

Figure 4.22: Schematic of the ON and OFF states of a liquid crystal display. Adapted from source unknown.

The left diagram in Fig. 4.22 represents the ON state of an LCD. Light comes from the bottom, and after crossing the first polariser it is fully polarised in the same direction as the

director of the liquid crystal. As ligth travels through the twisted nematic, it is rotated by 90°, and when it reaches the second polariser it is aligned with it, so it is fully transmitted.

The OFF state of an LCD is obtained by applying an electric field along the liquid crystal as shown in the right diagram in Fig. 4.22. The applied electric field leads to an induced electric dipole moment on the molecules due to charge separation, and the molecules distort to align with the applied field. However, the molecules near the edges are forced to retain their original configuration by the grooves on the contact surfaces. This structural transition driven by an applied electric field is called a *Fréedericksz transition*. In this configuration, light still comes from the bottom, and after crossing the first polariser it is fully polarised in the same direction as the director of the liquid crystal. However, light is no longer rotated as it travels through the liquid crystal as the sample exhibits no birefringence because the propagation direction of light is parallel to the director across most of the sample. As a result, no light is transmitted when it reaches the second polariser.

Overall, an electric field is used to switch the state of a pixel between ON and OFF as described above. Note that an LCD does not generate light, it either uses ambient light, in which case there is a mirror at the back to reflect the light, or it has an independent light source at its back. Colour LCDs use the same strategy described above, but also include colour filters to generate red, green, and blue pixels.

Appendix A

Gauss's law and parallel plate capacitors

This Appendix is non-examinable.

In electromagnetism, Gauss's law relates the distribution of electric charges Q to the resulting electric field $\mathbf{E}$:

$$\oint_S \mathbf{E} \cdot d\mathbf{A} = \frac{Q}{\varepsilon_0}. \tag{A.1}$$

This equation states that the electric flux through a closed surface S (left hand side) is proportional to the total charge Q enclosed by the surface (right hand side). The vector $\mathbf{A}$ is locally normal to the surface S. In the presence of a dielectric, Gauss's law can be equivalently written in terms of free charges Q_{free} and the displacement field $\mathbf{D}$:

$$\oint_S \mathbf{D} \cdot d\mathbf{A} = Q_{\text{free}}. \tag{A.2}$$

In a parallel plate capacitor context, the free charges are those on the conducting plates. By comparison, bound charges are those associated with the polarisation of the dielectric, which are "bound" to their local environment.

Consider a single infinite plane of charge density σ. Also consider a Gaussian surface S given by a cylinder symmetrically arranged about the infinite plane of charge:

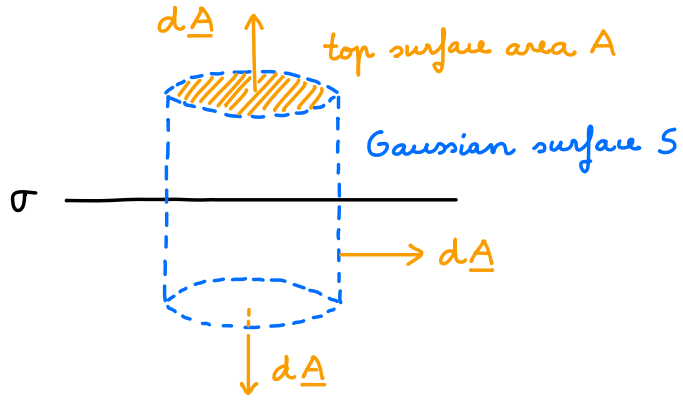

By symmetry, the displacement field $\mathbf{D}$ arising from the charge distribution is perpendicular to the plane, so for the vertical sides of the cylinder we have $\mathbf{D} \cdot d\mathbf{A} = 0$. Again by symmetry, the displacement field $\mathbf{D}$ has the same magnitude but opposite direction at the top and bottom circular surfaces of the cylinder, so that in both cases $\mathbf{D} \cdot d\mathbf{A} = |\mathbf{D}|dA$, where dA is the magnitude of the vector $d\mathbf{A}$. Applying Gauss's law as written in Eq. (A.2), the left hand side gives:

$$\oint_S \mathbf{D} \cdot d\mathbf{A} = \int_{\text{top surface}} |\mathbf{D}|dA + \int_{\text{bottom surface}} |\mathbf{D}|dA = 2|\mathbf{D}|A, \tag{A.3}$$

where in the last equality we have used the fact that $|\mathbf{D}|$ is constant across the surface. Finally, equating this expression to the right hand side of Eq. (A.2), we obtain:

$$|\mathbf{D}| = \frac{1}{2}\sigma \tag{A.4}$$

for an infinite plane of charge. This result implies that the displacement field arising from an infinite sheet of charge is constant and independent of the distance from the sheet.

We can model a parallel plate capacitor as two parallel sheets of charge, with equal magnitude charge densities σ but opposite sign charges:

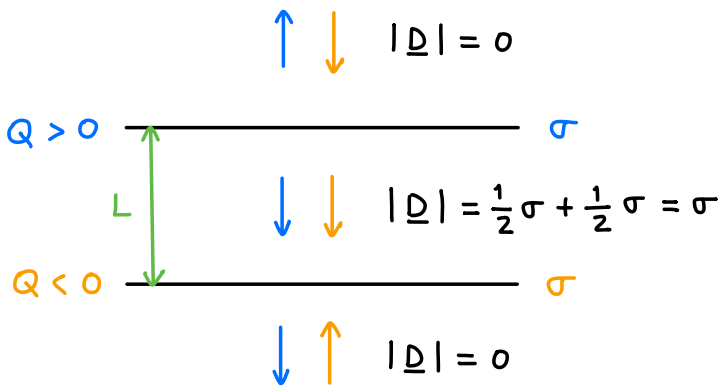

The blue arrows refer to the constant magnitude displacement field arising from the top infinite plane of positive charge, for which the displacement field direction points away from the plane. The orange arrows refer to the corresponding displacement field arising from the bottom infinite plane of negative charge, for which the field direction points towards the plane. In-between the two planes of charge the two displacement fields add up together, yielding $|\mathbf{D}| = \sigma$. Outside the two planes of charge the two displacement fields are in opposite directions and cancel, yielding $|\mathbf{D}| = 0$.

Overall, for a parallel plate capacitor the charge density on the plates is equal to the magnitude of the displacement field of the dielectric material between the plates, thus proving Eq. (1.10) in the main text, $\sigma = |\mathbf{D}|$.

Appendix B

Atomic origin of magnetism

This Appendix is non-examinable.

In quantum mechanics, electrons carry two types of angular momentum:

- Orbital angular momentum. This angular momentum is associated with the orbital motion of electrons and is the quantum mechanical version of the classical angular momentum.
- Spin angular momentum. This is an angular momentum of quantum mechanical origin that has not classical analogue and is associated with an intrinsic property of electrons (and other microscopic particles) called *spin*.

Angular momentum in quantum mechanics is quantised. This implies that its magnitude can only take a discrete set of values (rather than a continuum). For example, the magntidue of the spin angular momentum of electrons can only take the two values $\pm\frac{1}{2}\hbar$, where $\hbar = 1.054571817 \times 10^{-34}$ Js is called the reduced Planck constant.

Atoms are made of interacting electrons arranged in atomic shells and subshells as determined by the Pauli exclusion principle. For example, the hydrogen atom has an electron configuration $1s$, which means it has a single electron in shell 1 and subshell s. As another example, the carbon atom has an electron configuration $1s^2 2s^2 2p^2$, which means it has two electrons in each of the shell 1 subshell s, shell 2 subshell s, and shell 2 subshell p. In this context, filled electron shells have no net angular momentum, which implies that there is no magnetic moment associated with them. Partially filled shells do have a net angular momentum, which implies that they have an associated magnetic moment.

The magnetic moment of an atom arises from the combination of all angular momentum contributions, including the orbital and spin contributions from each electron. In this course, it can be useful to think about a magnetic material as made of individual magnetic moments, which can be roughly thought of in terms of individual atoms carrying magnetic moments. Reality is more complicated, for example there can be "itinerant" electrons that are not bound to any specific atom, which can lead to so-called "itinerant magnetism".

The quantum mechanics behind angular momentum and atomic structure are covered starting from Part IB, but if you are interested you can find the relevant content in our series of videos on angular momentum in quantum mechanics and on the hydrogen atom.

Appendix C

Order in nematic liquid crystals

This Appendix is non-examinable.

Consider a collection of rod-like molecules described as cylindrical and without internal structure. The probability of finding a molecule pointing in a an infinitesimal solid angle $d\Omega$ centred around (θ, ϕ) is:

$$f(\theta, \phi)d\Omega = f(\theta, \phi)\sin\theta d\theta d\phi, \tag{C.1}$$

where we are using the standard infinitesimals in spherical coordinates. For example, if all molecules are perfectly aligned along $\mathbf{D}$ (taken to be along the z axis without loss of generality), we get:

$$f(\theta, \phi)d\Omega = \begin{cases} \frac{1}{2} & \text{for } \theta = 0, \\ \frac{1}{2} & \text{for } \theta = \pi, \\ 0 & \text{otherwise.} \end{cases} \tag{C.2}$$

This expression can also be written more compactly as:

$$f(\theta, \phi) = \frac{1}{2\sin\theta}\left[\delta(\theta) + \delta(\theta - \pi)\right]\delta(\phi), \tag{C.3}$$

where $\delta(x)$ is the Dirac delta function. As a reminder, the Dirac delta function in one dimension is defined through this integral:

$$\int_{-\infty}^{\infty} dx f(x)\delta(x - x_0) = f(x_0), \tag{C.4}$$

and in three dimensions we can generalise this definition to:

$$\int_{-\infty}^{\infty} dx \int_{-\infty}^{\infty} dy \int_{-\infty}^{\infty} dz f(x, y, z)\delta(x - x_0)\delta(y - y_0)\delta(z - z_0) = f(x_0, y_0, z_0). \tag{C.5}$$

Using the standard rules of changes of variable, we can re-write the delta functions in spherical coordinates as:

$$\delta(x - x_0)\delta(y - y_0)\delta(z - z_0) = \frac{1}{r^2\sin\theta}\delta(r - r_0)\delta(\theta - \theta_0)\delta(\phi - \phi_0), \tag{C.6}$$

and this is the form used in Eq. (C.3).

As another example, if the molecules are randomly oriented, then the distribution function is constant because every direction is equally likely, and normalisation dictates that it takes the value:

$$f(\theta, \phi) = \frac{1}{4\pi}. \tag{C.7}$$

The order parameter Q from Eq. (4.14) can be written as:

$$Q = \frac{1}{2}\langle 3\cos^2\theta - 1\rangle = \frac{1}{2}\int d\Omega f(\theta, \phi)\left(3\cos^2\theta - 1\right). \tag{C.8}$$

If we start with fully aligned molecules, whose distribution is given by Eq. (C.3), we find:

$$\begin{aligned} Q &= \frac{1}{2}\int d\Omega \left[\frac{1}{2\sin\theta}\left[\delta(\theta)+\delta(\theta-\pi)\right]\delta(\phi)\right]\left(3\cos^2\theta-1\right) \\ &= \frac{1}{4}\int_0^{\pi} d\theta \sin\theta \int_0^{2\pi} d\phi\delta(\phi)\frac{1}{\sin\theta}\left[\delta(\theta)+\delta(\theta-\pi)\right]\left(3\cos^2\theta-1\right). \end{aligned} \tag{C.9}$$

The ϕ-integral gives 1, and we obtain:

$$Q = \frac{1}{4}\left[\int_0^{\pi} d\theta \left(3\cos^2\theta-1\right)\delta(\theta) + \int_0^{\pi} d\theta \left(3\cos^2\theta-1\right)\delta(\theta-\pi)\right]. \tag{C.10}$$

Each of the two θ-integrals inside the square brackets evaluates to 2, so we finally obtain:

$$Q = \frac{1}{4}(2+2) = 1. \tag{C.11}$$

Therefore, for fully aligned molecules the order parameter is $Q = 1$.

If we next consider randomly oriented molecules, whose distribution is given by Eq. (C.7), we find:

$$\begin{aligned} Q &= \frac{1}{2}\int d\Omega \left[\frac{1}{4\pi}\right]\left(3\cos^2\theta-1\right) \\ &= \frac{1}{8\pi}\int_0^{2\pi} d\phi \int_0^{\pi} d\theta \sin\theta \left(3\cos^2\theta-1\right). \end{aligned} \tag{C.12}$$

The ϕ-integral gives 2π, and we can separate the bracket into two terms to obtain:

$$Q = \frac{1}{4}\left[3\int_0^{\pi} d\theta \sin\theta\cos^2\theta - \int_0^{\pi} d\theta\sin\theta\right]. \tag{C.13}$$

Both integrals inside the square brackets are standard integrals, giving $\frac{2}{3}$ and 2 respectively, so we finally obtain:

$$Q = \frac{1}{4}\left(3\times\frac{2}{3}-2\right) = 0. \tag{C.14}$$

Therefore, for randomly oriented molecules the order parameter is $Q = 0$.